LBL--25261

DE88 010857

A Search for New Leptons with Heavy Neutrinos in e^+e^- Annihilation at $\sqrt{s} = 29$ GeV

Lisa Gay Mathis
Ph.D. Thesis

Department of Physics
University of California, Berkeley, CA 94720
and
Lawrence Berkeley Laboratory,
University of California, Berkeley, CA 94720

May 5, 1988

Abstract

This thesis describes the results of a search for new leptons with associated heavy neutrinos. The search uses 68.1 pb^{-1} of data taken with the TPC/2γ detector at the PEP storage ring. New lepton pairs with charged lepton masses $m_L < 12$ GeV and mass differences in the approximate range 0.4 GeV $< m_L - m_{\nu_L} < 2.5$ GeV are excluded at the 99% confidence level. Results are also given of a study of search techniques for the region $m_L < 12$ GeV, $m_L - m_{\nu_L} < 0.4$ GeV.

This work is supported by the United States Department of Energy under Contract DE-AC03-76SF00098

Contents

Acknowledgements

I would like, first of all, to acknowledge the many years of hard work of all the TPC/2γ people, past and present (and not only physicists). My work on the TPC has only been a very small addition to theirs. I thank my colleagues for friendly help and advice at every turn, and my friends for being friends. I thank my advisors Stu Loken and Roy Kerth for their help and encouragement, and for being people as well as physicists I could look up to. And I thank the state of California for its lonely beaches and grassy hillsides and the seals and deer who live there in a world of their own, and don't much care about physics.

Chapter 1

Introduction

1.1 Why Search for Leptons with Heavy Neutrinos?

Electrons have been recognized particles since the 1890's, muons were discovered in cosmic rays in 1936, and tau leptons were discovered in e^+e^- collisions in 1975[1]. These particles, their associated neutrinos, and the antiparticles of both form the three known families of leptons: spin 1/2 particles which interact weakly and electromagnetically, but not strongly. Are there any more leptons? This thesis describes one of the many searches that have been made for new leptons.

The masses of the known leptons are given in Table 1.1. It is not known why

$m_e =$	.511	MeV	$m_{\nu_e} <$	.000046 MeV
$m_\mu =$	105.66	MeV	$m_{\nu_\mu} <$	.25 MeV
$m_\tau =$	1784.2	MeV	$m_{\nu_\tau} <$	70. MeV

Table 1.1: Masses of known leptons

the charged lepton masses have these particular values, nor is it known whether the neutrinos have any mass at all. These are two basic particle physics questions still waiting to be answered. The fourth generation that is conventionally fit into the above pattern is a (L^-,ν_L) pair with $m_L \leq 100$ GeV and $m_{\nu_L} \approx 0$. Limits on such leptons have been set at both e^+e^- and $p\bar{p}$ colliders; the limits are $m_L > 21$ GeV and $m_L > 41$ GeV, respectively [2]. This doesn't mean there are no

new leptons with masses below the energies accessible with current experiments, however, only that if they exist they must fit into a different pattern. This is not a major drawback, since there is no strong theoretical argument favoring *any* pattern of lepton masses [3]. The problem is to choose which of the possible variations to search for. In the experiment described here, the choice was to allow the neutrino mass m_{ν_L} to have any value between zero and m_L, the mass of its charged partner, rather than assuming that m_{ν_L} is approximately zero. Lepton pairs of this type are of interest for two reasons:

1. If the mass difference $\Delta m \equiv m_L - m_{\nu_L}$ is less than about 3 GeV, the charged lepton would not have been found by past searches for fourth generation leptons, which assumed $m_{\nu_L} \approx 0$. This observation was first made by Perl in 1986[4], and is explained in more detail in the next section. In the absence of any accepted theory which predicts the masses of known and future neutrinos, allowing for the possibility of very massive neutrinos can be considered more the fixing of an oversight than an extension of the standard concept of leptons.

2. If the neutrino is close in mass to the charged lepton (within a few GeV) then according to a theory proposed in 1986 by Raby and West[5] it could have properties which would solve both the solar neutrino problem and the dark matter problem. The solar neutrino problem is that the measured number of neutrinos coming from the sun is less than the predicted number by a factor of three. The dark matter problem is that 90% of the mass in the universe is of an unidentified type whose existence has only been inferred from its gravitational effects. For the theory of Raby and West to work, m_{ν_L} must be between 4 GeV and 10 GeV, and there must also be another pair or triplet of new particles: $h^{\pm}$ and h^0 Higgs bosons.

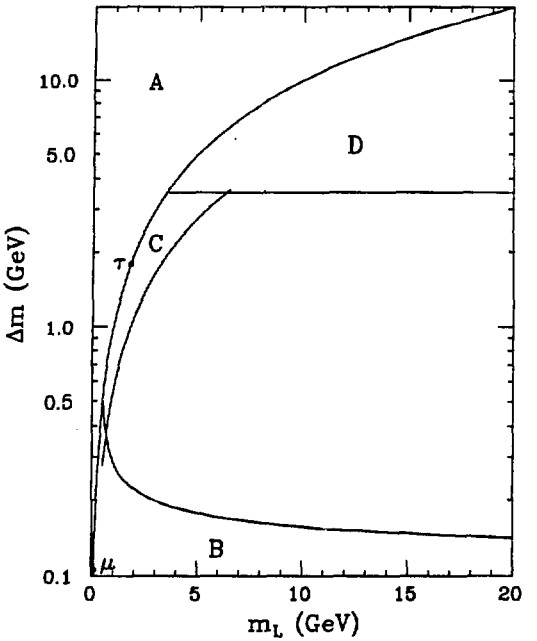

Figure 1.1: The mass difference, m_L- m_{ν_L}, vs the charged lepton mass, m_L, of possible lepton pairs. A fourth generation lepton pair is not allowed in Regions A, B, C and D.

1.2 Current Limits

Limits on a new pair of leptons could come from any of three categories: limits on new charged leptons, limits on new neutrinos, or limits on more exotic particles with similar properties. In addition, since 1986, data from two experiments (besides this one) have been reevaluated looking specifically for close-mass lepton pairs. These limits are explained below.

Figure 1.1 shows the status of limits on new leptons in 1986, as summarized

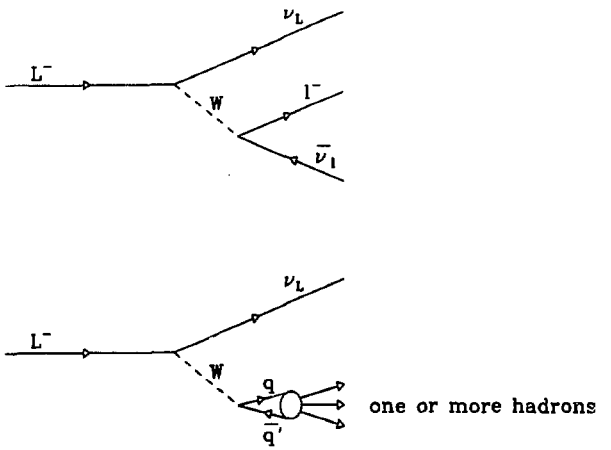

Figure 1.2: Leptonic and hadronic decays of charged heavy leptons.

by Perl. Region A is an unphysical region in which $m_L < 0$. Leptons with conventional massless neutrinos lie on the line bounding region A; no new leptons lie on this line below $m_{\nu_L} = 41$ GeV. In the region to the right of the line the 41 GeV limit doesn't apply, as explained below, except fairly close to the line (Region C) where ${m_{\nu_L}}^2 \leq 0.2{m_L}^2$[4]. A JADE experiment[6], searching for supersymmetric charginos decaying weakly to massive photinos, excludes the possiblility of leptons with $m_L < 22.5$ GeV and $\Delta m > 3.5$ GeV, Region D. Searches for stable charged leptons[7], have excluded approximately Region B, which is bounded by the line where the mean flight length is 1 meter for leptons with PETRA's 22.5 GeV beam energy.

To see why the possibility of $m_{\nu_L} > 0$ affects the limits on m_L, it is necessary to consider how the limits are set. Charged leptons which are associated with lighter neutrinos decay weakly as in Figure 1.2, either to hadrons or to pairs

of lighter leptons. Both the decay rate and the relative probabilities of the decay modes are primarily determined by $\Delta m = m_L - m_{\nu_L}$. For the tau, with $\Delta m = m_\tau = 1.784$ GeV, the lifetime is $c\tau = .01$ cm, the decays to $e^-\overline{\nu}_e\nu_L$ and $\mu^-\overline{\nu}_\mu\nu_L$ each have branching fractions of 17-18%, and the remaining 65% of the decays are to one or a few hadrons. In the limit of very high Δm, the lifetime approaches zero, and the branching fractions are expected to be roughly 10% each to $e^-\overline{\nu}_e$, $\mu^-\overline{\nu}_\mu$, and $\tau^-\overline{\nu}_\tau$, and 35% each to large numbers of hadrons via $\overline{u}d$ or $\overline{u}s$, and $\overline{c}s$ or $\overline{c}d$. In searches for new charged leptons with massless neutrinos, $\Delta m = m_L$ and so is always greater than m_τ. The searches therefore look for the new leptons through their decays, and usually look for at least one decay to a jet of hadrons, to maximize the number of possible events[8,9,10]. (A MARKJ search looked only for two muons, but required them to have momenta greater than 9 GeV[11].)

The possibility of massive neutrinos allows Δm to be much smaller, with the result that the probability of hadronic decays, particularly to jets rather than to a single hadron, may be much less than expected. In addition, because the massive neutrinos carry away most of the energy, the maximum visible energy of the events will be much smaller. The searches typically make a cut against low visible energy events to reduce background, or require high-energy acoplanar tracks: either requirement would remove possible small-Δm events. (This is the reason, for example, that heavy leptons would not have shown up in measurements of $\tau^+\tau^-$ cross sections.) The lower-than-expected multiplicity and visible energy of the events is why current e^+e^- lower limits on m_L don't apply when $m_{\nu_L} \not\approx 0$.

There is also a $p\overline{p}$ limit $m_L > 41$ GeV from UA1[12]. This experiment looked for $W^+ \rightarrow L^+\nu_L$; $L^+ \rightarrow \overline{\nu}_L q\overline{q}'$ (or the charge conjugate reaction), which appears in a $p\overline{p}$ experiment as an event with large unbalanced transverse energy. If the neutrinos are massive, however, the missing energy is large but approximately

balanced; it is estimated that lepton pairs are not excluded by this search when $\Delta m \leq 0.6\, m_L$[13].

The best limits on possible new neutrinos come from single-photon experiments at e^+e^- colliders, which look for the process $e^+e^- \rightarrow \gamma\nu\overline{\nu}$ by detecting a lone photon. These experiments give a combined limit of (number of ν types) < 4.8[14]. These searches are relatively insensitive to neutrino mass, but they require $m_{\nu_L} \leq (E_{beam} - \frac{1}{2}E_\gamma)$, where E_{beam} is either 14.5 GeV or 21.3 GeV, and E_γ must be large enough to allow $p_\perp(\gamma) \geq 1$ to 4 GeV. The limit thus applies only to neutrinos with m_{ν_L} less than about 12 GeV.

Limits from $p\overline{p}$ experiments are comparable [15,16] and extend to higher neutrino masses, but are more model dependent. The most recent UA2 limit, from a measurement of Γ_Z/Γ_W, is (number of ν types) < 3 to 7, depending on the mass of the top quark. (This limit explicitly assumes that neither Z's nor W's decay to any other new particle. If the decays $Z \rightarrow L^+L^-$ and $W \rightarrow L\nu_L$ are included, the bounds are slightly higher[17].) Neither e^+e^- nor $p\overline{p}$ experiments, therefore, exclude a fourth generation of leptons.

The present status of limits on heavy leptons is shown in Figure 1.3. Region E is bounded by the estimated UA1 limit mentioned above. Mark II has extended the limits to lower Δm by looking for (low-energy) e-μ, e-jet, and μ-jet pairs[18]. Their search excludes new leptons in Region F.

1.3 Future Limits

The results of the study described in this thesis reduce further the m_L,Δm region where new leptons are allowed. But since there is still a region open to them, they may still exist (elusively). It is therefore comforting to know that finding them or excluding them should be less difficult with the next generation of detectors. The searches as very small Δm will be helped by the increase with higher energies

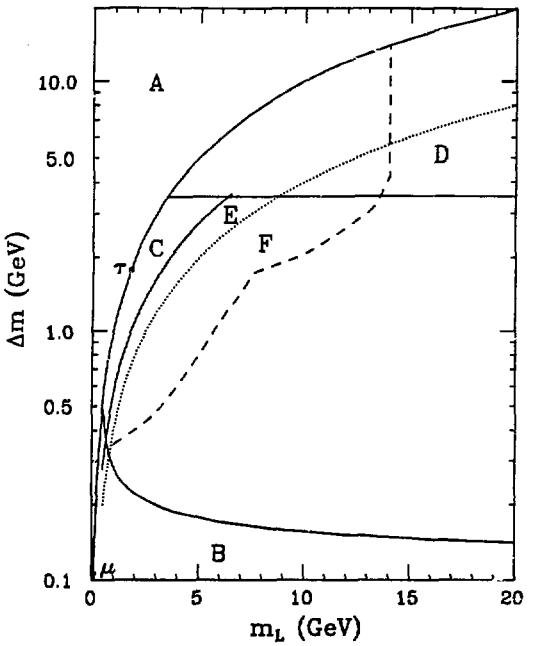

Figure 1.3: The mass difference vs charged lepton mass of possible lepton pairs. Region E is excluded by $p\bar{p}$ limits on new leptons with massless neutrinos, and Region F by a study of Mark II data.

of the mean flight distance of the charged leptons. Searches for new "stable" particles and searches which look for decays away from the vertex will both work better, especially for those detectors which include vertex detectors. The experiments at LEP and SLC will also be able to search all of the m_L,Δm range, for m_L up to 50 GeV, by measuring the number of neutrino generations. By again looking for $e^+e^- \rightarrow \gamma\nu\overline{\nu}$, but this time at $\sqrt{s} \geq m_Z$ where the cross section is much higher, it's estimated that the existence of a fourth neutrino family can be confirmed or excluded at the 5σ level after one month of data-taking at LEP (at a luminosity of $10^{31}\text{cm}^{-2}\text{sec}^{-1}$)[19]. If no fourth neutrino is found, a close-mass lepton generation with $m_L \leq \frac{1}{2}m_Z$ will be excluded as well. Of course, if a fourth neutrino *is* found, we will have to continue to look for a possible charged lepton partner.

Chapter 2

The Physics of Heavy Leptons

The first step in looking for a new particle is to predict what its properties would be. In the case of new leptons these properties can for the most part be predicted with confidence, once it is assumed that the new leptons are just like known leptons except for their masses. Exactly what assumptions are made is explained in Section 2.1. The important properties to know are how the leptons are produced, and if and how they decay. These are explained in Sections 2.2 - 2.4.

2.1 Assumptions

The heavy leptons considered here are called sequential leptons. This means that they are assumed to belong to a pair (L^-,ν_L) of leptons which has its own strictly conserved lepton number. In addition, the neutrino mass is allowed to be non-zero, but is assumed to be less than the lepton mass. These two assumptions together mean that the only possible decays are the weak decays $L^- \rightarrow \nu_L X^-$ of Figure 1.2 (or the charge conjugates).

The three known neutrinos ν_e, ν_μ, and ν_τ are given zero mass in all calculations, and it is assumed that there is no mixing between neutrinos of different generations, in particular between the ν_L and any lighter ν. This is implied by the conservation of lepton number, and ensures that the ν_L will be stable.

The heavy lepton L is assumed to have the same electromagnetic and weak coupling as the e, μ, and τ. This is:

$$\bar{\psi}\gamma^{\mu}\left[eQA_{\mu}+\frac{g(1-\gamma_5)}{2\sqrt{2}}\left(T^{+}W_{\mu}^{+}+T^{-}W_{\mu}^{-}\right)+\frac{g}{\cos\theta_W}\left(\frac{1}{2}(1-\gamma_5)T_3-\sin^2\theta_W Q\right)Z_{\mu}\right]\psi$$

where $\psi=\begin{pmatrix}\nu_L\\ L^-\end{pmatrix}$. In decays, only the weak charged current part of the coupling is involved, and the coupling reduces to $-i(g/\sqrt{2})\bar{u}_{\nu}\gamma^{\mu}\frac{1}{2}(1-\gamma_5)u_L$ for L^- decays, and $-i(g/\sqrt{2})\bar{v}_L\gamma^{\mu}\frac{1}{2}(1-\gamma_5)v_{\nu}$ for L^+ decays, where u and v are four component Dirac wavefunctions. This is the standard vector-axial vector "V-A" interaction. No possibility of a different mixture of vector and axial vector couplings is considered.

Sometimes lepton families with massless neutrinos are written as $\begin{pmatrix}\nu_L\\ L^-\end{pmatrix}_L+(L^-)_R$. There is however no problem for the standard model in changing the leptons from a left-handed doublet $(\nu_L,L^-)_L$ and right-handed singlet $(L^-)_R$ to two doublets $(\nu_L,L^-)_L$ and $(\nu_L,L^-)_R$. The left and right "handedness" is *defined* by $\frac{1}{2}(1-\gamma_5)\begin{pmatrix}\nu_L\\ L^-\end{pmatrix}=\begin{pmatrix}\nu_L\\ L^-\end{pmatrix}_L$. This means $\frac{1}{2}(1-\gamma_5)\begin{pmatrix}\nu_L\\ L^-\end{pmatrix}_R=0$, so although the coupling now contains terms like $-i(g/\sqrt{2})W_{\mu}^{+}(\bar{\nu})_R\gamma^{\mu}\frac{1}{2}(1-\gamma_5)(L^-)_R$, such terms always vanish. The effect of the neutrino mass is not to introduce right-handed couplings, but rather (since handedness and helicity are identical only for massless particles) to introduce couplings to positive helicity neutrinos.

Finally, in the branching ratio calculations only decays to known particles are included. In particular it is assumed that there is only *one* new lepton pair and the possibility of decay modes such as Figure 2.1(a) is not allowed for. Possible decays to other new particles (Figure 2.1(b)) such as the associated Higgs particle postulated in the theory of Raby and West[5] are also not considered.

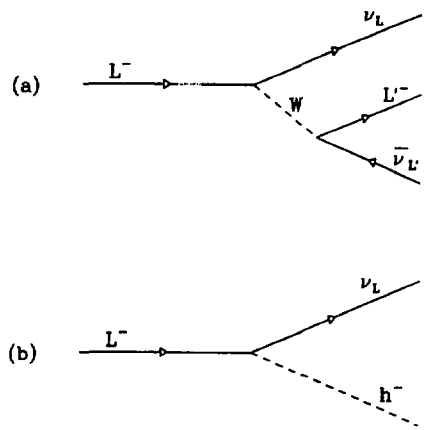

Figure 2.1: Two examples of heavy lepton decays which were not allowed for in the calculation of branching fractions.

2.2 Production Cross Section, and Radiative Corrections

The lowest order cross-section for lepton production in e^+e^- annihilation is:

$$\sigma^0_{L^+L^-} = \sigma^0_{\mu^+\mu^-}\frac{\beta(3-\beta^2)}{2},$$

where $\sigma^0_{\mu^+\mu^-} = 4\pi\alpha^2/3s$ is the cross section for muon pair production (in the approximation that muons are massless), $s = (2E_{beam})^2$ is the square of the center of mass energy, and β is the velocity of the leptons.

The differential cross section is :

$$\frac{d\sigma}{d\Omega} = \frac{\alpha^2}{4s}\beta[1+\cos^2\theta+(1-\beta^2)\sin^2\theta],$$

where θ is the angle between the produced leptons and the beamline. Figure 2.2 shows this cross section for leptons with masses between 2 and 14 GeV and PEP's 14.5 GeV beam energy.

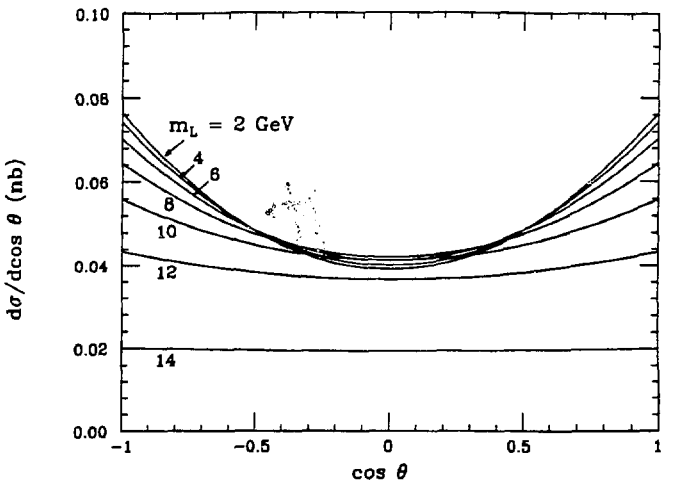

Figure 2.2: The dependence of the lepton production cross section on the angle between the leptons and the beamline, for several lepton masses, and with a beam energy of 14.5 GeV.

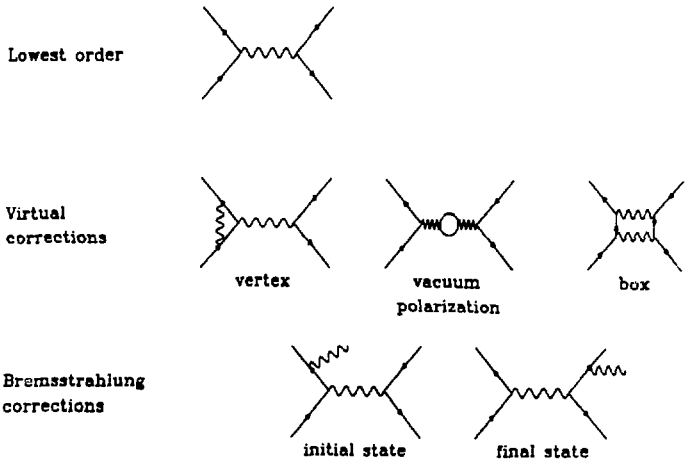

Figure 2.3: Processes included in the calculation of radiative corrections.

First order radiative corrections come from the processes shown in Figure 2.3[20]. They change both the total lepton pair cross section and the momentum distributions of the leptons. In calculations of radiative corrections, the Bremsstrahlung contribution is usually divided into soft and hard radiation. The contribution from the soft photons is then combined with the virtual contributions and evaluated analytically. The division point (in photon energy) is arbitrary and is typically chosen so that the soft photons are uninteresting experimentally. Above this point, the differential cross-section for the hard photons is integrated over phase space and added to the analytic correction to give the total correction. This approach has the advantage that it is easily adapted for use in Monte Carlo simulations of lepton production.

In these calculations the approximation is often made that the masses of both

the initial and final state leptons are much less than the beam energy. A second common approximation is to neglect the effects of final state radiation on the total cross-section. This approximation was originally made so that the resulting corrections could be applied also to production of quark pairs, for which the final state correction was unknown or model-dependent[21]. It is justified by the observation that the final state contribution to the cross section is small when $m_L/E_{beam} \ll 1$.

A calculation without the approximation that $m_L/E_{beam} \ll 1$ has also been done[22]. The result is an expression for the correction which is a sum of three terms: $\sigma_{total} = \sigma^0_{total}(1 + \delta_{VP} + \delta_{ini} + \delta_{fin})$. Here, δ_{VP} is the vacuum polarization correction, δ_{ini} is the correction from initial state radiation and virtual soft photons, and δ_{fin} is from final state radiation.

Table 2.1 gives the total cross sections, calculated in these three ways, for some real and hypothetical leptons. The analysis described later always uses the non-approximate cross sections.

m_L (GeV)	σ^0	σ (approx)	δ_{VP}	δ_{ini}	δ_{fin}	σ (no approx)
.106	.103	.165	.100	.495	.002	.165
1.784	.103	.136	.100	.219	.002	.136
2.	.103	.135	.100	.208	.002	.135
4.	.103	.128	.100	.136	.002	.128
6.	.102	.123	.100	.087	.003	.122
8.	.099	.119	.100	.043	.004	.114
10.	.093	.114	.100	-.005	.007	.102
12.	.078	.108	.100	-.073	.012	.081
14.	.039	.094	.100	-.238	.036	.035

Table 2.1: Radiatively corrected cross sections for lepton production (in nb).

2.3 Branching Fractions and Lifetimes

Leptons with conserved lepton number must decay weakly to lepton or quark pairs (as in Figure 1.2). The theory of weak decays tells, as well as possible, how

to calculate the rates Γ_i of possible decay modes[23,24,25,26]. The branching fraction to each mode i is then given by $B_i = \Gamma_i/\Gamma_{total}$, and the lifetime of the lepton is $\tau = 1/\Gamma_{total}$.

2.3.1 Decay Rates

The rates of weak decays to leptons are exactly calculable with the standard model of weak interactions. For the hadronic decays the theory is less certain. The decay products are anything the quarks can form, most commonly some number of charged and neutral pions, with the choice being dependent on q^2, the mass of the virtual $W^{\pm}$ (and this in turn determines the q^2 distribution of the decays). At low q^2 the hadronization is strongly affected by resonances, so calculations of decay rates to π, K, ρ, K^* and a_1 are done explicitly. When the mass difference Δm between the lepton and its neutrino is large, high q^2 decays must also be included, for which the hadronization is less predictable. The high q^2 decay rates are estimated by calculating to rate of decays to quark pairs in the limit of infinite q^2, and then requiring that the decay rates approach this limit along smooth curves which are also required to give the correct branching fractions for tau decay when $\Delta m = m_L = m_\tau$.

For the purposes of calculation, then, the decays are divided into one leptonic and three hadronic classes: scalar, vector, and (vector) continuum. In each case, the decay rate is given by:

$$d\Gamma_i = \frac{1}{2m_L} \mid M_i \mid^2 dQ,$$

where $M_i = (4G_F/\sqrt{2}) J_L^\mu J_{\mu,i}^\dagger$ is the invariant amplitude and dQ is the phase space term: $dQ = (2\pi)^4 \delta^4(p - p_1 - \cdots p_n) \prod_{i=1}^n d^3p_i/(2\pi)^3 2E_i$. The heavy lepton part of the current is the same for all four classes:

$$J_L^\mu = \bar{u}_{\nu_L} \gamma^\mu \tfrac{1}{2}(1 - \gamma^5) u_L \,.$$

For the other currents, examples for the four classes are:

$$\begin{aligned} J^{\dagger}_{\mu,e} &= \overline{u}_e \gamma_\mu \tfrac{1}{2}(1-\gamma^5) v_{\nu_e} \\ J^{\dagger}_{\mu,\pi} &= \tfrac{1}{2} f_\pi \cos\theta_c q_\mu \\ J^{\dagger}_{\mu,\rho} &= \tfrac{1}{2} g_\rho \cos\theta_c \epsilon_\mu \\ J^{\dagger}_{\mu,\overline{u}d} &= \tfrac{1}{2} c_{\overline{u}d} \cos\theta_c \epsilon_\mu . \end{aligned}$$

In all, twelve decay rates are calculated: three leptonic modes $e^-\overline{\nu}_e\nu_L$, $\mu^-\overline{\nu}_\mu\nu_L$ and $\tau^-\overline{\nu}_\tau\nu_L$, two scalar modes $\pi^-\nu_L$ and $K^-\nu_L$, three vector (or axial vector) modes $\rho^-\nu_L$, $K^{*-}\nu_L$ and $a_1^-\nu_L$, and four continuum modes $\overline{u}d\nu_L$, $\overline{u}s\nu_L$, $\overline{c}s\nu_L$ and $\overline{c}d\nu_L$. In the rest of this discussion the decays to $e^-\overline{\nu}_e\nu_L$, $\pi^-\nu_L$, $\rho^-\nu_L$ and $\overline{u}d\nu_L$ will be used to represent the four classes; within each class the results for the other modes can always be obtained by simple substitutions of coupling constants, factors of $\cos\theta_c$ and $\sin\theta_c$, and final state masses.

The coupling constants for the hadronic modes come from a combination of experiment and theory[24,27]: f_π and f_K from π and K decay, g_ρ from $e^+e^- \to \rho \to \pi^+\pi^-$, g_{K^*} from g_ρ and SU(3) symmetry, and g_{a_1} from $\tau^- \to a_1^-\nu_\tau$. The values used in this calculation are: $f_\pi = .132$, $f_K = .159$, $g_\rho = .165$, $g_{K^*} = .191$, and $g_{a_1} = .300$. The continuum coupling is $c_{\overline{u}d} = c_{\overline{u}s} = c_{\overline{c}s} = c_{\overline{c}d} = 1$. The cosine of the Cabbibo angle θ_c gives the correct likelihood of producing a pair of quarks from the same generation, and is $\cos\theta_c = .975$.

The Γ_i are evaluated by squaring the matrix elements M_i and, for the hadronic modes, integrating $d\Gamma_i$ over all variables except q^2 (where q is the four-momentum of the $W^\pm$). (The leptonic integral is different as explained below.) In the case that $m_{\nu_L} = 0$, this gives:

$$\begin{aligned} \Gamma_{L^- \to e^-\overline{\nu}_e\nu_L} &= \frac{1}{96\pi^2}\Gamma_0 \frac{1}{m_L^6} \\ &\times \int (m_L^2 - m_e^2 - 2m_L E_{\nu_e}) m_L E_{\nu_e} \delta\left[(p_L - p_e - k_{\nu_e})^2\right] \frac{d^3p_e}{2E_e}\frac{d^3k_{\nu_e}}{2E_{\nu_e}} \end{aligned}$$

$$\Gamma_{L^-\to\pi^-\nu_L} = 12\pi^2 f_\pi^2 \cos^2\theta_c \Gamma_0 \frac{1}{m_L^8} \times \int_0^{m_L^2} m_L^2(m_L^2-q^2)^2 r_\pi(q^2)dq^2$$

$$\Gamma_{L^-\to\rho^-\nu_L} = \frac{12\pi^2 g_\rho^2 \cos^2\theta_c}{m_\rho^2}\Gamma_0 \frac{1}{m_L^2} \times \int_0^{m_L^2} (m_L^2+2q^2)(m_L^2-q^2)^2 r_\rho(q^2)dq^2$$

$$\Gamma_{L^-\to\overline{u}d\nu_L} = 6c_{\overline{u}d}^2 \cos^2\theta_c \Gamma_0 \times \int_0^{m_L^2} (m_L^2+2q^2)(m_L^2-q^2)^2 r_{\overline{u}d}(q^2)dq^2.$$

In these and later equations, $\Gamma_0 = G_F^2 m_L^5/192\pi^3$ is the rate of the decay $L^- \to e^-\overline{\nu}_e\nu_L$ when $m_{\nu_L} = 0$. $\Gamma_0 = (1/1.595 \times 10^{-12}\text{sec})$ when $m_L = m_\tau$.

The leptonic expression could also be written as an integral over dq^2, but q^2 isn't a very useful variable in this case because $|M|^2$ is proportional to $(p_{\nu_L} \cdot p_e)(p_L \cdot p_{\nu_e})$ and so the momenta of the three final state particles are correlated and there is no simple dependence on q^2. This would be true for all the hadronic decays as well if they were calculated according to the quark diagram of Figure 1.2.

The factors $r_i(q^2)$ are included in the integrals to give the resonant q^2 dependence of the decays. For the three hadronic currents, the forms used for $r_i(q^2)$ are:

$$r_\pi(q^2) = \delta(q^2-m_\pi^2)$$

$$r_\rho(q^2) = (m_\rho\Gamma_\rho/\pi)/\left[(q^2-m_\rho^2)^2+\Gamma_\rho^2 m_\rho^2\right]$$

$$r_{\overline{u}d}(q^2) = \theta(q^2-\Lambda_{\overline{u}d}^2).$$

The expression for $r_\rho(q^2)$ is a Breit-Wigner resonance form and Γ_ρ is the width of the decay of the ρ (not of the decay *to* the ρ). For the three vector modes, the widths used were $\Gamma_\rho = .153$ GeV, $\Gamma_{K^*} = .051$ GeV, and $\Gamma_{a_1} = .316$ GeV. In the expression for $r_{\overline{u}d}(q^2)$, $\Lambda_{\overline{u}d}$ is a somewhat arbitrary low-q^2 cutoff parameter, below which the rates are dominated by resonant decays[28]. In this calculation, $\Lambda_{\overline{u}d} = \Lambda_{\overline{u}s} = 1.1$ GeV, and $\Lambda_{\overline{c}d} = \Lambda_{\overline{c}s} = 2$ GeV.

For $m_{\nu_L} \neq 0$, the equations for Γ_i must be generalized by keeping terms

containing m_{ν_L} when calculating the Γ_i. The expressions then become:

$$\begin{aligned}
\Gamma_{L^-\to e^-\overline{\nu}_e\nu_L} &= \frac{1}{96\pi^2}\Gamma_0\frac{1}{m_L^6}\times\int(m_L^2-m_e^2-m_{\nu_L}^2-2m_LE_{\nu_e})m_LE_{\nu_e} \\
&\quad \delta\left[(p_L-p_e-p_{\nu_e})^2-m_{\nu_L}^2\right]\frac{d^3p_e}{2E_e}\frac{d^3p_{\nu_e}}{2E_{\nu_e}} \\
\Gamma_{L^-\to\pi^-\nu_L} &= 12\pi^2f_\pi^2\cos^2\theta_c\Gamma_0\frac{1}{m_L^8} \\
&\times \int_0^{(m_L-m_{\nu_L})^2}\Delta^{1/2}\left[(m_L^2-m_{\nu_L}^2)^2-q^2(m_L^2+m_{\nu_L}^2)\right]r_\pi(q^2)dq^2 \\
\Gamma_{L^-\to\rho^-\nu_L} &= \frac{12\pi^2g_\rho^2\cos^2\theta_c}{m_\rho^2}\Gamma_0\frac{1}{m_L^2} \\
&\times \int_0^{(m_L-m_{\nu_L})^2}\Delta^{1/2}\left[(m_L^2-m_{\nu_L}^2)^2+q^2(m_L^2+m_{\nu_L}^2)-2q^4\right]r_\rho(q^2)dq^2 \\
\Gamma_{L^-\to\nu_L\overline{u}d} &= 6c_{\overline{u}d}^2\cos^2\theta_c\Gamma_0 \\
&\times \int_0^{(m_L-m_{\nu_L})^2}\Delta^{1/2}\left[(m_L^2-m_{\nu_L}^2)^2+q^2(m_L^2+m_{\nu_L}^2)-2q^4\right]r_{\overline{u}d}(q^2)dq^2,
\end{aligned}$$

with $\Delta \equiv m_L^4+m_{\nu_L}^4+q^4-2m_L^2m_{\nu_L}^2-2m_L^2q^2-2m_{\nu_L}^2q^2$.

At this point, the calculation of the Γ_i is well-defined and can be done numerically. In practice, however, some of the expressions have more compact (but less easy to interpret) forms which are the algorithms actually used in the software. For the leptonic decay, if two of the three final state particles are massless,

$$\Gamma_{leptonic} = \Gamma_0(1-8\eta^2+8\eta^6-\eta^8-12\eta^4\ln\eta^2),$$

with $\eta = m/m_L$ where m is the non-zero mass[24]. This is used for decays to $e^-\overline{\nu}_e\nu_L$ (setting $m_e=0$), or if $m_{\nu_L}=0$. For most cases there's only one massless final state particle (the light neutrino) and then the formula is[29]:

$$\begin{aligned}
\Gamma_{leptonic} &= \Gamma_0\times\frac{1}{2}\left[2-3s^3-s^2+(5D-14)s-13D\right]r \\
&\quad -\frac{3}{2}\left[s^4-2(D+2)s^2+D^2-4D\right]L_1+12s\sqrt{D}L_2,
\end{aligned}$$

with the definitions $m_l = m_\mu$ or m_τ, $s=(m_{\nu_L}^2+m_l^2)/m_L^2$, $D=\left[(m_{\nu_L}^2-m_l^2)/m_L^2\right]^2$, $r=\sqrt{1-2s+D}$, $L_1=\ln[(1-s+r)/(2m_lm_{\nu_L}/m_L^2)]$, and $L_2=\ln\left[(s-D-r\sqrt{D})/(2m_lm_{\nu_L}/m_L^2)\right]$.

For the scalar decays, $r(q^2)$ is a delta function so the integral can be done easily and the result is just the replacement everywhere of q^2 by m_π^2 or m_K^2.

The vector decay rate is integrated numerically, with the additional requirement that $q^2 \geq (2m_\pi)^2$ for decays to ρ, $q^2 \geq (m_\pi + m_K)^2$ for decays to K^*, and $q^2 \geq (3m_\pi)^2$ for decays to a_1 (so as to ensure a possible decay mode for the resonance).

For the hadronic continuum the expression for Γ can be integrated analytically[30], to give :

$$\begin{aligned}\Gamma_{L^- \to \overline{u}d\nu_L} &= 6c_{\overline{u}d}^2 \cos^2\theta_c \Gamma_0 \, 4\eta \left[\eta\left(-\frac{2\sin\theta_\Lambda}{\cos^4\theta_\Lambda} - \frac{\sin\theta_\Lambda}{\cos^2\theta_\Lambda} + 3\ln\left|\sec\theta_\Lambda + \tan\theta_\Lambda\right|\right)\right. \\ &\quad \left. + 2\sqrt{\eta}(1+\eta)\tan^3\theta_\Lambda\right]\end{aligned}$$

with $\eta = m_{\nu_L}^2/m_L^2$, $x_\Lambda = \Lambda_{\overline{u}d}^2/m_L^2$, $\sec\theta_\Lambda = (1+\eta-x_\Lambda)/(2\sqrt{\eta})$ and $0 \leq \theta_\Lambda \leq \pi/2$.

These expressions give, for τ^- decays, the branching fractions $e^-\overline{\nu}_e\nu_\tau(17.8\%)$, $\mu^-\overline{\nu}_\mu\nu_\tau(17.4\%)$, $\pi^-\nu_\tau(10.8\%)$, $K^-\nu_\tau(0.7\%)$, $\rho^-\nu_\tau(22.0\%)$, $K^{*-}\nu_\tau(1.1\%)$, $a_1^-\nu_\tau$ (12.5%), $\overline{u}d\nu_\tau(16.7\%)$, and $\overline{u}s\nu_\tau(0.9\%)$. The agreement between these fractions and the measured tau branching fractions was arranged by adjusting the two least well-determined parameters: $\Lambda_{\overline{u}d}$ and g_{a_1}.

2.3.2 Branching ratios

For a lepton pair with a given m_L and Δm, the branching fractions are $B_i = \Gamma_i/\Gamma_{total}$, where $\Gamma_{total} = \sum_i \Gamma_i$ is the total decay rate for the lepton. These fractions depend strongly on Δm, and only very weakly on m_L. Figure 2.4 gives the fractions as a function of Δm for an example with $m_L = 10$ GeV. As an example of the m_L dependence, for $\Delta m = 1$ GeV the branching fraction for $L^- \to \pi^-\nu_L$ is .232 at $m_L = 2$ GeV and .221 at $m_L = 14$ GeV.

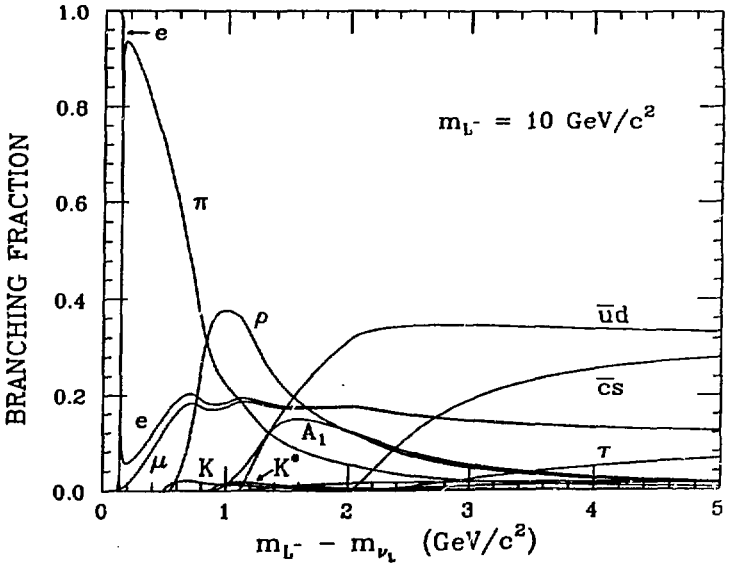

Figure 2.4: Probabilities of ten decay modes, for leptons with $m_L = 10$ GeV and a range of m_{ν_L}. The branching fractions for other m_L are only slightly different.

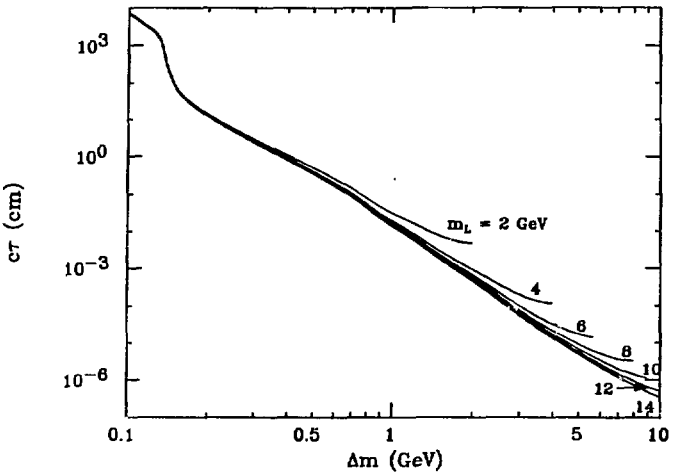

Figure 2.5: Predicted lifetimes of new leptons as a function of $m_L - m_{\nu_L}$, for seven lepton masses, m_L.

2.3.3 Lifetimes

The lifetimes of the heavy leptons, given by $c\tau = c/\Gamma_{total}$, are also primarily dependent on Δm. This dependence is shown in Figure 2.5. For experiments, the important number is not the lifetime but the mean flight distance $x_0 = \beta\gamma c\tau$, where $\beta\gamma = p_L/m_L$. For a fixed beam energy the flight distance depends on both m_L and Δm. Curves showing this dependence for $E_{beam} = 14.5$ GeV are given in Figure 6.1 of Chapter 6.

2.4 Angular correlations

Lepton pairs produced in e^+e^- collisions have correlated spins. The general rule is that the spins tend to be parallel to each other. If m_L/E_{beam} is small, helicity

is conserved and the spins also tend to be parallel or anti-parallel to the direction of the leptons, while if $m_L/E_{beam} \approx 1$, angular momentum is conserved and the spins stay parallel to the beamline.

If $\vec{s}$ and $\vec{s}'$ are the spin vectors of the L^+ and L^- in their rest frames, and θ is the angle between $\vec{p}_{L^-}$ and $\vec{p}_{e^-}$, the dependence of the L^+L^- cross section on spins is given by[23]:

$$\begin{aligned}\frac{d\sigma}{d\Omega}(\vec{s},\vec{s}') &= \frac{\alpha^2}{16s}\beta\left[1+\cos^2\theta+\frac{\sin^2\theta}{\gamma^2}+s_z s_z'\left(1+\cos^2\theta-\frac{\sin^2\theta}{\gamma^2}\right)\right.\\ &\left.+s_x s_x'\left(1+\frac{1}{\gamma^2}\right)\sin^2\theta-s_y s_y'\beta^2\sin^2\theta+(s_x s_z'+s_x' s_z)\frac{1}{\gamma}\sin 2\theta\right],\end{aligned}$$

where s is the center of mass energy squared and $1/\gamma = m_L/E_{beam}$.

The importance of this spin correlation lies in the fact that lepton decays are anisotropic: the distributions of the decay products depend on the direction of the spin of the lepton parent. The correlation between the L^+ and L^- spins therefore introduces a correlation between the decay products.

The rule for decay correlations is that negative leptons prefer to go opposite to the spin of their parents, while positive leptons go parallel. For pions the rule is reversed: negative pions prefer to be parallel to the L^- spin, and positive pions go antiparallel. (Decays to more than one pion are more complicated and less strongly correlated.) The decay cross sections can all be written in the form:

$$\frac{d\Gamma}{d\Omega} \propto 1+\alpha\cos\phi$$

where ϕ is the angle between the lepton spin and the daughter electron or pion. In the case that $m_{\nu_L} = 0$, $\alpha = \pm 1$ for $\pi^{\mp}$, and $\alpha = \mp(2x-1)/(3-2x)$ for $e^{\mp}$, where $x = E/E_{max}$, E is the electron energy, and $E_{max} = m_L/2$. For the electrons, the maximum correlation is when $x = 1$.

For $m_{\nu_L} \geq 0$, the corresponding expressions are:

$$\alpha_{\pi^{\mp}} = \pm\frac{(p_{\nu_L}/E_{\nu_L})(m_L^2-m_{\nu_L}^2)(m_L^2+m_{\nu_L}^2-m_\pi^2)}{(m_L^2-m_{\nu_L}^2)^2-m_\pi^2(m_L^2+m_{\nu_L}^2)}$$

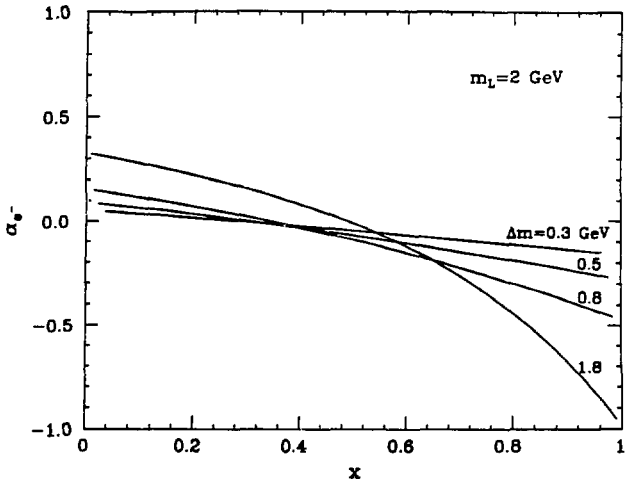

Figure 2.6: The ratio of the spin-correlated decay rate to the isotropic decay rate for the decay $L^- \to e^- \overline{\nu}_e \nu_L$, as a function of the ratio x of the electron energy to its maximum allowed value. The curves shown are for $m_L = 2$ GeV; for heavier leptons and the same values of Δm, the correlation is weaker.

for pions, and

$$\alpha_{e^\mp} = \pm \frac{(1-x)f - (m_L/E_{max} + 1 - 2x)\frac{1}{2}f^2 + (m_L/E_{max} - x)\frac{1}{3}f^3}{(1-x)f + (2x-1)\frac{1}{2}f^2 - \frac{1}{3}xf^3}$$

for electrons[27], with $x = E/E_{max}$, $E_{max} = (m_L^2 - m_{\nu_L}^2)/2m_L$, and $f = 1 - (m_{\nu_L}^2/m_L(m_L - 2E))$.

For both electron and pion decays, the correlation is weaker when the ν_L is massive, but for pions it's only slightly weaker and can be approximated as $\alpha_{\pi^\mp} = \pm 1$. The electron decays are more complicated. To give a feeling for the strength of the correlation, Figure 2.6 gives $\alpha_{e^-}(x)$ for $m_L = 2$ GeV and a range of m_ν, while Figure 2.7 gives α_{e^-} as a function of $\Delta m = m_L - m_{\nu_L}$ for some values of m_L and with $x = .999$.

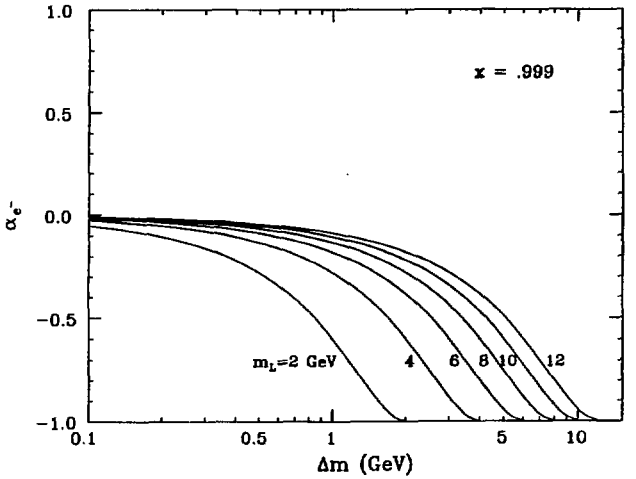

Figure 2.7: The ratio of the spin-correlated decay rate to the isotropic decay rate for the decay $L^- \to e^- \overline{\nu}_e \nu_L$, as a function of $m_L - m_{\nu_L}$, for six values of m_L. The curves show the maximum correlation, which occurs when the electron has its maximum possible energy ($x = 1$).

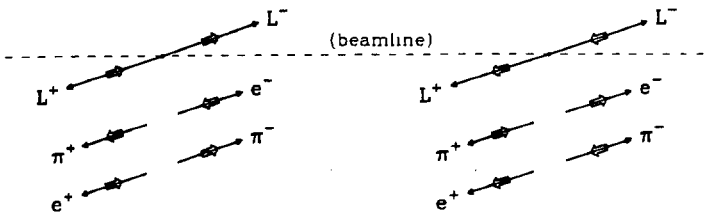

Figure 2.8: Favored directions for electrons and pions from decays of pairs of heavy leptons. The directions are shown in the rest frames of the heavy leptons.

The combination of spin-spin and spin-decay angle correlations is shown pictorially in Figure 2.8. The directions of the pions and electrons are shown in the rest frame of their parents. This rest frame correlation of the directions is translated into momentum correlations in the lab frame.

Chapter 3

TPC Data

The search for heavy leptons described in this thesis uses data from two years of running the TPC/2γ detector at the Stanford Linear Accelerator Center (SLAC). The detector is located in one of the interaction regions of SLAC's electron-positron storage ring, PEP, and was designed and is used to study the results of e^+e^- collisions. The characteristics of the data are determined by three things: the physics of e^+e^- collisions (what actually happens), the kind and quality of information that the detector can provide, and the selection of which events to record. These are described in the next three sections.

3.1 PEP, and e^+e^- Physics

PEP is a 700 meter diameter ring in which three bunches of 14.5 GeV electrons circulate clockwise, and three 14.5 GeV positron bunches circulate counterclockwise. At six points (interaction regions) along the ring, two bunches cross every 2.44 μsec. The size of the beams and their positioning determine the rms distance of each interaction from the average interaction point: about .01 cm vertically and .05 cm horizontally perpendicular to the beam, and 1.5 cm along the beam. The typical luminosity of the beams is $1-2\times10^{31}\mathrm{cm}^{-2}\mathrm{sec}^{-1}$ ($.01-.02\,\mathrm{nb}^{-1}\mathrm{sec}^{-1}$); the integrated luminosity for the TPC/2γ data-taking from 1984 to 1986 was 68.1 pb^{-1}.

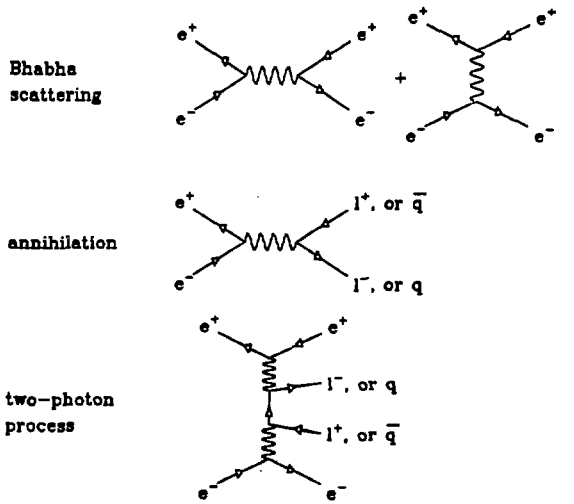

Figure 3.1: Common processes in e^+e^- collisions.

When an electron and positron collide, one of three things usually happens. Either they exchange a photon and scatter, or they annihilate and produce a pair of new particles, or each emits a photon and the two photons interact. Figure 3.1 shows the Feynman diagrams for these three processes, and Figure 3.2 shows some of their cross sections as a function of beam energy[31,32]. The annihilation and two-photon cross-sections have been further sub-divided depending on the types of the particles produced. From this figure it can be seen that the most common event is a pair of leptons, either with fairly low energy from the predominantly low invariant mass two-photon events, or each with the beam energy. The hadronic events which are of the most interest (because they involve physics not completely understood) are relatively rare.

In addition to e^+e^- events, there are two kinds of background events which

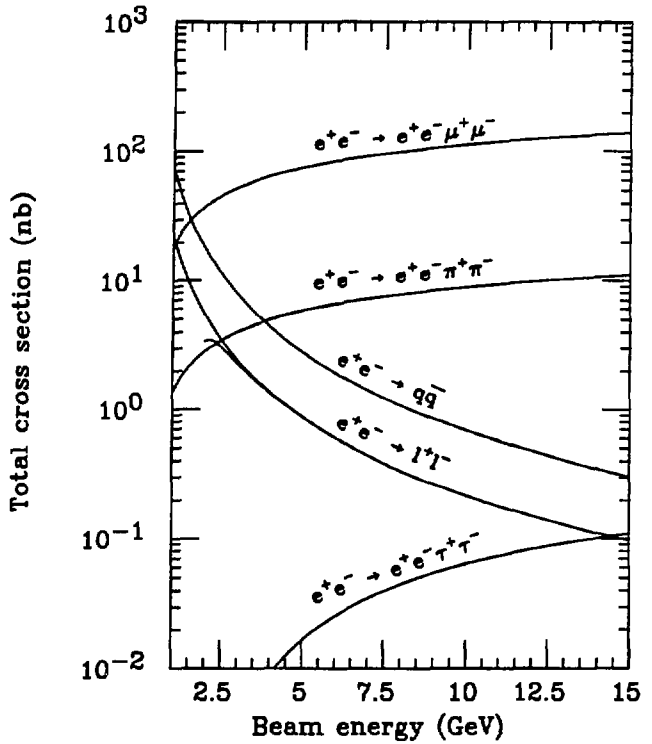

Figure 3.2: Total cross sections for some annihilation and two-photon processes, as a function of the beam energy (calculated to lowest order). The cross section for the two-photon process $e^+e^- \to e^+e^-e^+e^-$ is 8×10^5 nb at $E_{beam} = 14.5$ GeV.

are included in the data. One is beam gas events, in which an e^+ or e^- interacts with an atom in its path and the results scatter into the detector. The second is cosmic rays, of which about $2\,\mathrm{sec}^{-1}$ pass within 10 cm of the interaction point.

3.2 The Detector

The task of the detector is fairly well defined: it is to detect and identify all the particles leaving the interaction point in each event, determine where they originate, and measure the direction and magnitude of their momentum. This is usually accomplished by combining many detector subsystems each specialized for certain particle types or energies. The TPC/2γ detector, the central part of which is shown in Figure 3.3, is a good example of this technique. For this analysis, three of its subsystems were used; they and the characteristics of the information they provide are described below.

3.2.1 The TPC

The Time Projection Chamber (TPC), our central tracking detector, has the geometry shown in Figure 3.4. It has 55 kV/m electric and 13.2 kG magnetic fields parallel to each other and to the beamline, and is filled to 8.5 Atm with a mix of 80% argon and 20% methane. A charged particle, passing through the TPC in about 3 ns, leaves a track of ionization electrons along its path which then drift slowly (at 3.50 cm/μsec) along the electric field to the ends of the cylinder. The ends, each one divided into six sectors, are covered with wires and pads, as shown for one of the sectors in Figure 3.5. ("Pads" are isolated squares in the grounded cathode plane behind the wires.) Ionization electrons drifting in initiate electron avalanches in the large electric field around the wires which are then collected by the wires. Their positions along the wires are determined from the signals picked up capacitively by the nearest pads, and the time of

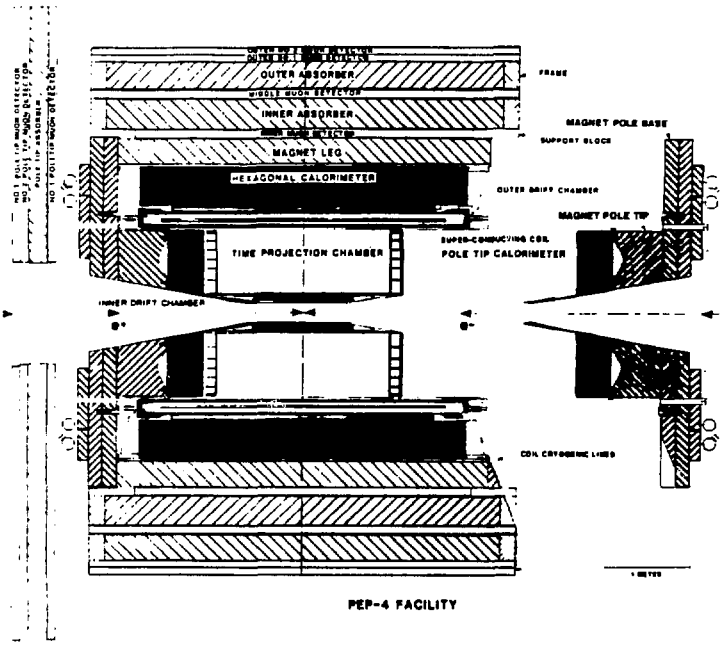

Figure 3.3: Central part of the TPC/2γ detector.

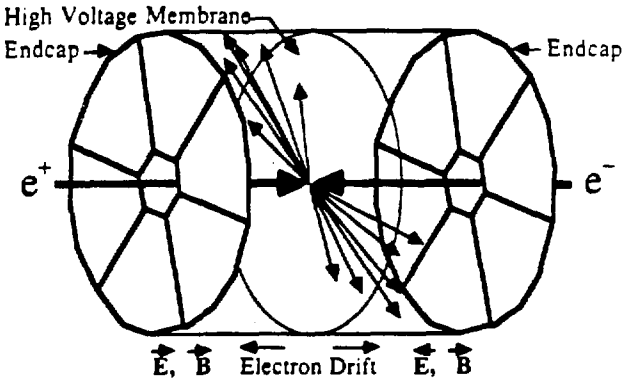

Figure 3.4: Schematic drawing of the time projection chamber (TPC).

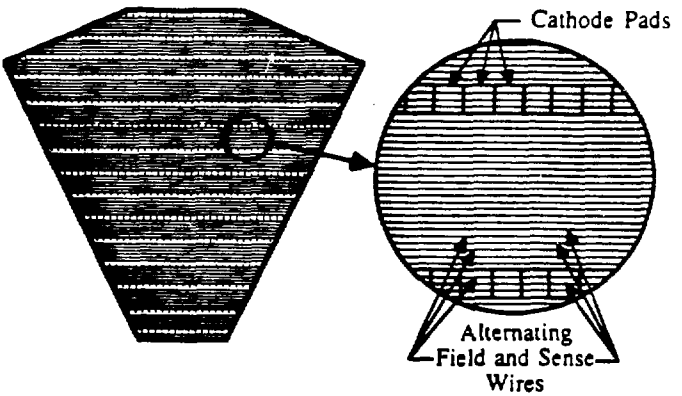

Figure 3.5: TPC sector showing the arrangement of the sense and field wires, and of the 15 pad rows.

their arrival gives the z-coordinate of the track at the radius of each wire. So by recording the ionization arriving at each wire and near each pad as a function of time (in 100 ns bins), the TPC records 183 2-dimensional and 15 3-dimensional points along a typical track. The ionization is amplified proportionally, so these 198 points are also measurements of the ionization density along each track. In this way, with a minimum of instrumentation, the TPC provides more than enough information for unambiguous track-finding, good particle identification, and high-level triggering.

The complete details of TPC construction, calibration, operation, and performance have been described elsewhere[33]. What is given here is a brief description of how the recorded pad and wire information is transformed into "TPC data" as used by the trigger and in analysis.

1. *Tracking.* Tracks are found in the TPC by fitting helices to the (3-dimensional) pad hits. The need for at least three points to determine a helix is the basic constraint on the track-finding efficiency. A second constraint is that the choice of helices to try is somewhat biased towards finding tracks from the vertex. (Not all helices are tried.) The result is that tracks are essentially always found as long as they come from near the interaction point and cross more than four or five pad rows. The most important acceptance problem is the loss of tracks which have dip angles greater than about 60° because they leave the TPC before crossing more than a couple of pad rows (The dip angle is defined as the angle of the track from the midplane.) Other, less numerous, lost tracks include straight tracks whose projection onto the endplane happens to fall along a boundary between sectors, low energy tracks which circle back into the beampipe before crossing enough pad rows, very low energy tracks (usually δ-rays) created in the TPC which spiral along the field lines, and tracks which are

short because they either begin or end in the TPC volume.

Figure 3.6 shows the wire and pad data for an event in which five low angle tracks and part of a spiraling track were missed. Although in this case the wire data clearly could be used to supplement the pad hits in the tracking algorithm, in most cases it has not been needed.

2. *Momentum measurement.* After the tracks are found, the helix fit to them is refined by adjusting the assignment of pad hits to the tracks, by weighting the measured points with the correct errors, and by making corrections for known (slight) distortions of the paths of the drifting ionization electrons. If the track comes from near the vertex, a fit is also done which includes the vertex point. The transverse momentum of the track is then proportional to the radius of curvature of the fitted helix, and the measured dip angle gives p_z. In the TPC's 13.2 kG magnetic field, $R_c = 253 p_\perp$ cm/GeV. The momentum resolution is $(\sigma_p/p)^2 = (.015)^2 + (.011p)^2$ (p in GeV) without a vertex constraint, and $(\sigma_p/p)^2 = (.015)^2 + (.007p)^2$ with the vertex constraint.

3. *Particle identification.* Identification of charged particles in the TPC depends on measuring the ionization density along their paths. This can also be expressed as energy loss per unit length (dE/dx), and for a given gas mixture, pressure and temperature depends only on the particle velocity. The velocity and momentum together identify the particle.

   Because the energy loss distribution has large fluctuations and a long tail of high energy losses, the best particle identification is achieved by calculating a "truncated mean" energy loss for each track. This is defined to be the mean of the 65% of the measurements with the lowest energy loss. References to the "dE/dx" of a TPC track almost always refer to this truncated

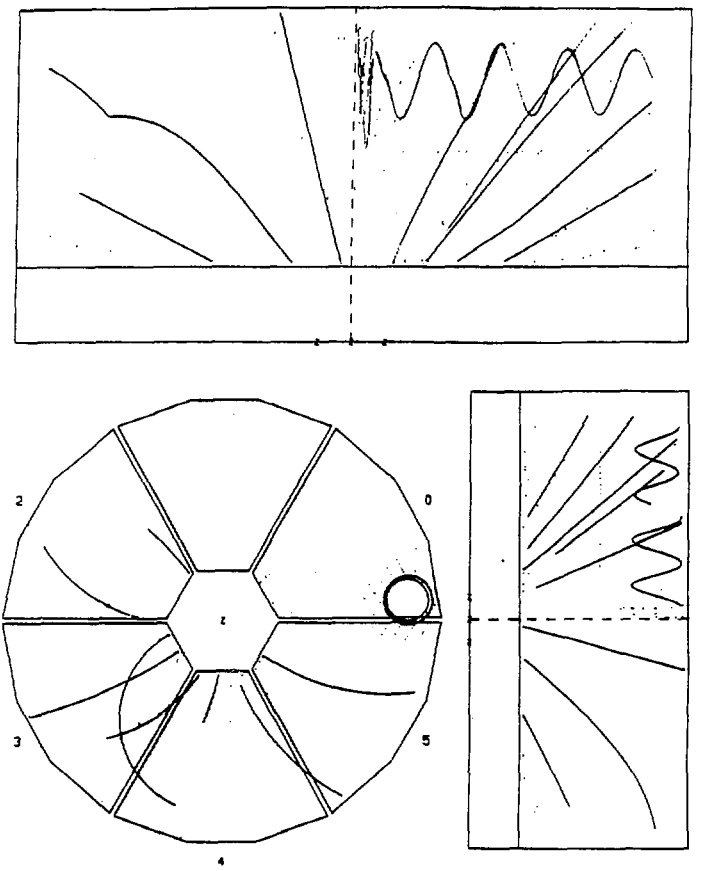

Figure 3.6: TPC data for a $q\bar{q}$ event. At the top is an r vs z plot of the wire hits, while the lower two diagrams show the pad hits. The solid lines are the fitted tracks.

mean. In the TPC, it is measured with a resolution of between 4% and 6% for most tracks (depending on the number of wires hit).

Figure 3.7 shows the predicted dE/dx as a function of momentum for the five charged particle species which are long-lived enough to be common in the TPC. A sample of data is also shown; for many tracks there is no doubt as to their identity. For every track, its momentum and dE/dx are used to define five "dE/dx χ^2" values, measuring consistency with the five particle types. For most analysis problems, tracks of specific particle species are selected by making cuts on these five dE/dx χ^2's.

4. *Triggering.* TPC wire hits are used by the trigger as a source of information on the dip angle and z-position of tracks. (Pad hits are not used because good azimuthal information is available from the drift chambers.) For the trigger, adjacent sectors are paired to form twelve 120° "supersectors" (six for each end). The supersectors overlap so that a track which crosses a sector boundary will still be completely within a supersector. Within each supersector the wires are grouped into twenty-three sets of eight adjacent wires. The hits in these groups form the TPC trigger signals.

3.2.2 Drift Chambers

There are two cylindrical drift chambers[34], one at the inner radius of the TPC and one just outside the superconducting magnet coil at the TPC's outer radius. No information from the drift chambers is associated with the tracks and used in the analysis, but the pattern of drift chamber hits is an important part of the trigger.

The Inner Drift Chamber (IDC) is 117 cm long (114.3 cm wire length), with four concentric layers of 60 sense wires each, at radii of 14.87, 16.07, 17.27 and 18.47 cm. Layers and cells within layers are separated only by field wires, with

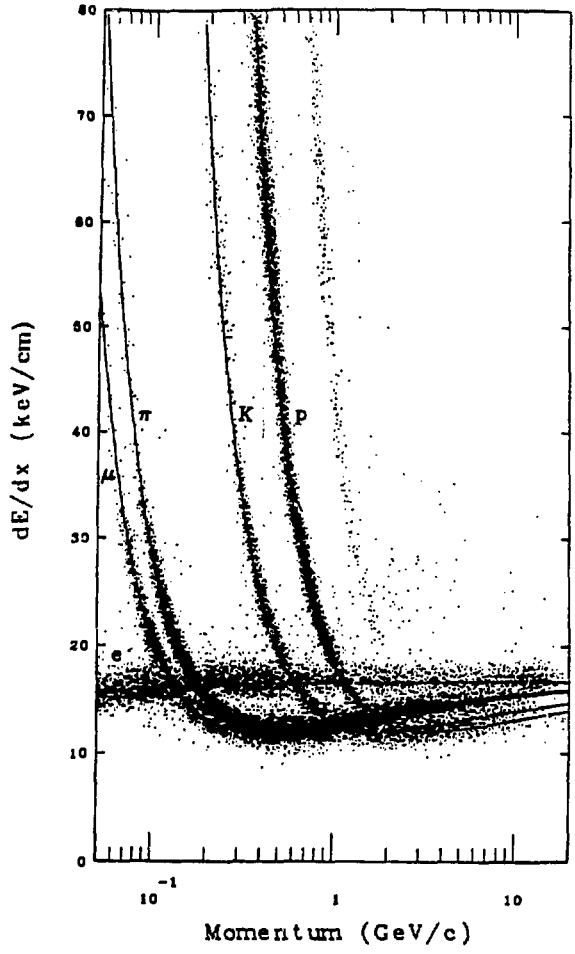

Figure 3.7: Measured dE/dx and momentum of a sample of TPC tracks, and curves of predictions for the five common particle types. (A deuteron band can also be seen to the right of the proton band.)

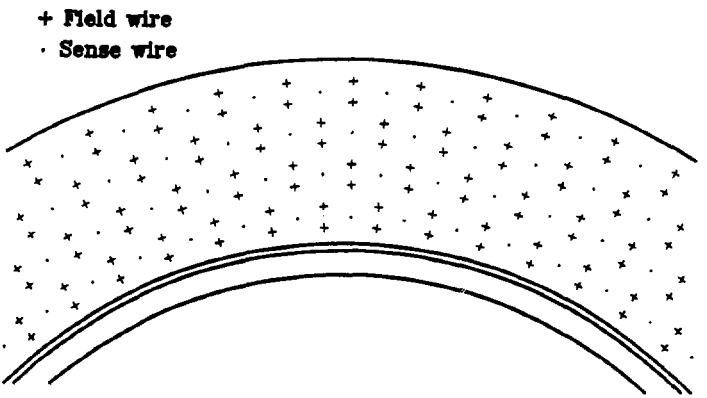

Figure 3.8: A 60° section of the inner drift chamber, with the wires and the beamline perpendicular to the page.

alternate layers offset by 3°. A section of the IDC is shown in Figure 3.8. It is filled with 80% Ar- 20% CH_4 at TPC pressure (8.5 Atm). All four layers can detect tracks with polar angles between 18° and 90°, giving a solid angle coverage of 95% of 4π.

The ODC is a 305 cm long cylinder (300 cm wire length) with three layers of 216 wires each, at radii of 119.7, 121.7 and 123.7 cm. The layers are offset as shown in Figure 3.9, with the cells separated by plastic I-beams. The ODC is filled with 1 Atm of 80% Ar- 20%CH_4. It will detect tracks between 40° and 90° (77% of 4π solid angle), with an efficiency of about 85% in each layer. Additional losses of low momentum tracks because of interactions in the .87 radiation length magnet coil also affect the probability of detecting them with ODC.

When the drift chambers are used by the trigger, the wires are grouped into 60 IDC "elements" and 72 ODC "elements". Figure 3.10 shows how they are defined. An element is hit if wires in two of its layers are hit. For the ODC any

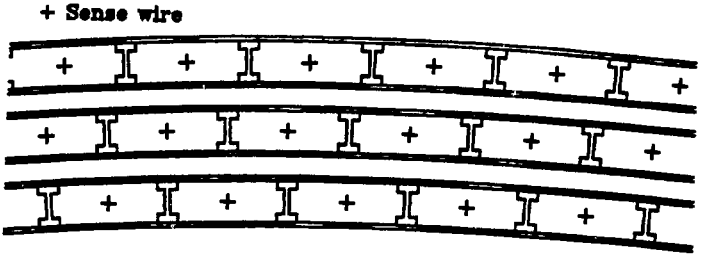

Figure 3.9: A 10° section of the outer drift chamber.

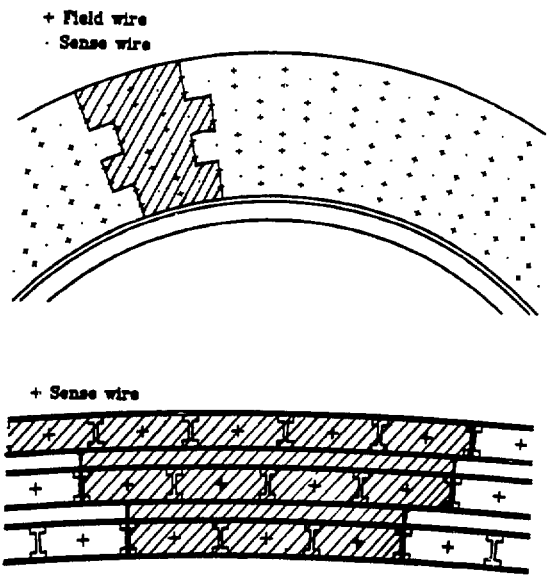

Figure 3.10: Definitions of IDC and ODC elements used in the trigger.

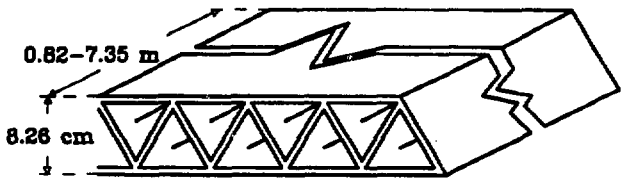

Figure 3.11: Part of a layer of muon chambers, showing the triangular cell structure.

two layers are allowed; in the IDC there must be a hit in either the A or C layer and one in either the B or D layer, and in addition the timing of the hits must be such that the sum of the drift times in two azimuthally offset layers is 180 ± 40 ns, where 180 ns is the maximum possible drift time. This is a way of selecting radial tracks[35].

3.2.3 Muon Chambers

The muon chambers[36] are the outermost part of the central detector. There are four layers in a hexagonal geometry surrounding the HEX calorimeter, and three layers covering each end, outside the Poletip calorimeter. Each layer is made of triangular tubes as in Figure 3.11; this gives them good (99%) efficiency for seeing at least one hit in each layer. They run on 1 Atm of 80% Ar- 20%CH_4. The drift times are read out for every hit, but only the wire locations are currently used in the analysis.

Tracks reaching the outermost layer of the muon chambers are filtered through between 4 and 11 interaction lengths of hadron absorber, mostly iron, depending on the angle of the track as shown in Figure 3.12. This means that muons with momenta below 2 GeV will not reliably reach the outer layer, and that about 1% of hadrons above 2 GeV *will* reach the outer layer. Therefore in a $q\bar{q}$

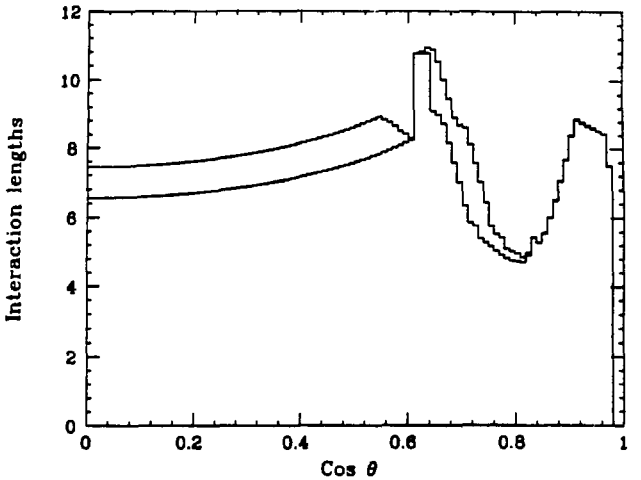

Figure 3.12: Interaction lengths before the outer layer of muon chambers, as a function of the cosine of the angle from the beamline. The number of interaction lengths also varies with azimuth; minimum and maximum values are shown.

environment, where hadrons outnumber the muons by over 30 to 1, the result is a 30% background in the "muon" sample. The high efficiency of the muon chambers makes them very effective however in *rejecting* muons down to energies of about 1 GeV, with the loss of only a small percentage of non-muons.

In the analysis, all tracks found in the TPC with momentum above 1 GeV are extrapolated out through the muon chambers, and any hits near them (within 6σ, where σ is the extrapolated measurement error) are assigned to them. Other muon chamber hits are ignored. Thus the muon chambers are not used for tracking but only to confirm or reject the particle identification of known TPC tracks.

3.3 The Trigger

At PEP, as in many colliding beam experiments, beam crossovers occur at a higher rate than the interactions of interest, and also at a much higher rate than that at which the data can be stored, or even collected. In our experiment, there are crossovers every 2.44 μsec, the drift time of tracks in the TPC is 30 μsec, and readout (storage) time is 100 msec. Fast (trigger) electronics is therefore used to survey the signals from the fastest parts of the detector and decide after each beam crossing whether to continue the readout[37]. The decision is made in three stages: the pre-pretrigger decides whether to reset the detector before the next beam crossing, the pretrigger decides whether to wait for tracks to drift completely in to the TPC endplanes, and the trigger decides whether to read out the event. Figure 3.13 gives a picture of the relationship between the data and the timing of the trigger.

To trigger on the different types of events of interest, several sets of trigger requirements were defined; only one set had to be satisfied to generate a trigger. For data-taking in 1984-86, four types of charged trigger (using the drift chambers

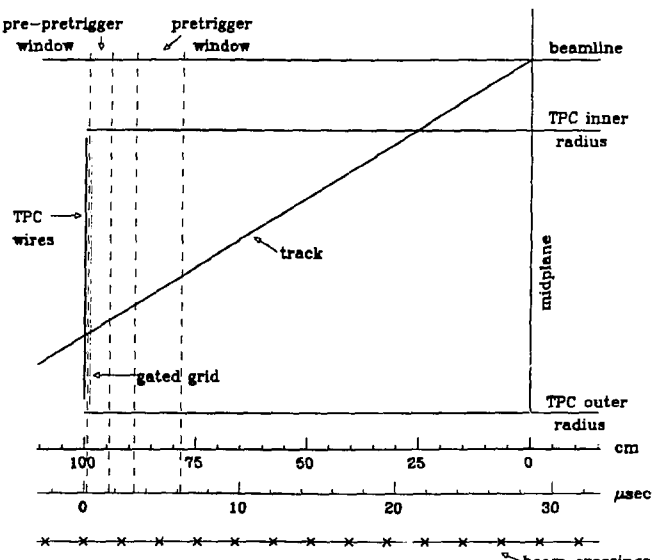

Figure 3.13: Timing of the pretrigger and pre-pretrigger. The axis in cm shows the track position in the TPC, while the axis in μsec gives the arrival time at the TPC wires of ionization electrons from the track.

and the TPC) and three types of neutral trigger (using the calorimeters as well) were allowed. The rest of this section focuses on the charged particle triggers, since they are the most suitable for detecting heavy lepton events. (Searches usually concentrate on the charged tracks because heavy lepton events always have at least two charged particles but not necessarily any neutral energy other than undetectable neutrinos.) Section 3.3.1 gives a more detailed description of the elements that make up a charged particle trigger, and Section 3.3.2 explains how the trigger requirements affect the trigger efficiency for low multiplicity events. These acceptance calculations are done only to give a general understanding of what kinds of events could be present in the data. In practice, the trigger efficiency is corrected for in the analysis by running all Monte Carlo events through a trigger simulation. The simulation is described briefly in Section 3 of the next chapter.

3.3.1 Trigger requirements

The four charged triggers are called the ripple, colinearity, coplanarity and majority triggers. All four are intended to trigger on events with two (or more) good tracks. The most important is the ripple trigger.

For the ripple trigger, the IDC and ODC elements are each grouped into 30° sections; their relation to the TPC supersectors is shown in Figure 3.14. A drift section chamber is hit if any of its elements are hit. For each TPC supersector, three signals are defined using the hits in its 23 wire groups (defined in Section 3.2.1). A hit on any wire in any group during the pre-pretrigger window is a TPCE signal, and four wires hit at once in any one of the outer 17 groups during the pretrigger window is a TPCF signal. Finally, there is a ripple in a supersector if there is a series of groups hit at consecutively smaller radii, and with timing which is consistent with hits from a track coming from the vertex.

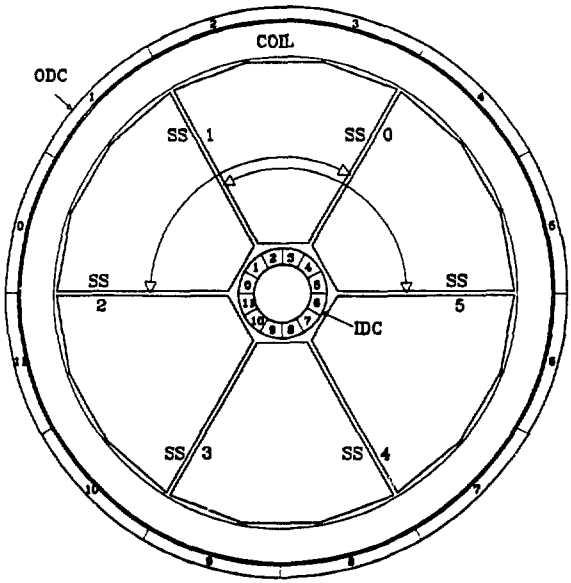

Figure 3.14: The major IDC, ODC and TPC trigger elements.

Next, coincidences between these groups are defined. There is considered to be an IDC-ODC coincidence at position i ($i = 0, 11$), if ODC section i is hit and IDC_{i-1}, IDC_i or IDC_{i+1} is hit. There is a TPCF coincidence in supersector i when there is a TPCF signal in that supersector and a hit in either of the two IDC sectors centered on it. For example, SS0 and IDC_1 or IDC_2. Similarly, a TPCS signal can only occur if there is a TPCF signal in the same supersector, or an IDC-ODC coincidence for one of the two ODC sectors centered on it.

The minimum requirements for the three stages of a ripple trigger then are:

1. *Pre-pretrigger.* Two IDC sections hit (separated by two or more IDC sections), and either any ODC section hit, or two IDC-TPCE coincidences.

2. *Pretrigger.* Two IDC-ODC coincidences (with no separation requirement), or one IDC-ODC coincidence and one IDC-TPCF coincidence, or two IDC-TPCF coincidences separated by at least one supersector.

3. *Trigger.* Two TPCS "ripples", separated by at least one supersector.

The coplanarity, colinearity and majority triggers differ from the ripple trigger because they require only one "ripple". Instead they make tighter azimuthal cuts. They are mostly used to provide backup triggering for events in which the hits from one track don't properly meet the definition of a ripple. Because most heavy lepton events are not particularly colinear or coplanar, only the ripple trigger was used in this study.

3.3.2 Trigger acceptance

For high multiplicity events, such as $q\bar{q}$ events, the trigger types are mostly redundant: usually several of them are satisfied and the resulting trigger efficiency is over 99%. In particular, the requirements of the charged particle triggers for two acceptable tracks are usually satisfied by several pairs of tracks in a high

multiplicity event. Rejection by the trigger logic or loss due to inefficiency of a single track is unimportant. In two-track events, however, there is often no redundancy. Both tracks must satisfy all the trigger requirements to generate a trigger. Some of the restrictions this places on tracks are given below.

1. *Minumim transverse momentum.* There are four ways in which a track may have a minumum transverse momentum requirement imposed on it.

   (a) If an ODC element is required, a track must have a large enough radius of curvature to reach the ODC. In the TPC's 13.2 kG field, the corresponding minumum $p_\perp$ is 241 MeV (to reach the middle layer of the ODC).

   (b) For tracks at large angles from the beam the requirement of an IDC-ODC coincidence translates into a minimum $p_\perp$ in the range 261 to 425 MeV, depending on the azimuth of the track.

   (c) For small angle tracks, the IDC-TPCF coincidence requirement requires $p_\perp > 85$ to 115 MeV, again depending on azimuth. The triggering efficiency for such tracks also depends on p_z: tracks with the minimum $p_\perp$ must be at their maximum radius when they reach the TPC endplane.

   (d) The IDC meantiming window of 180 ± 40 ns imposes a curvature constraint which translates into a $p_\perp$-min of about 100 MeV.

   Figure 3.15 shows examples of tracks which just meet the various minimum $p_\perp$ requirements.

2. *Maximum dip angle.* Tracks at small angles from the beamline must cross the TPC sectors at $r > 48$ cm, corresponding to a dip angle of 64°.

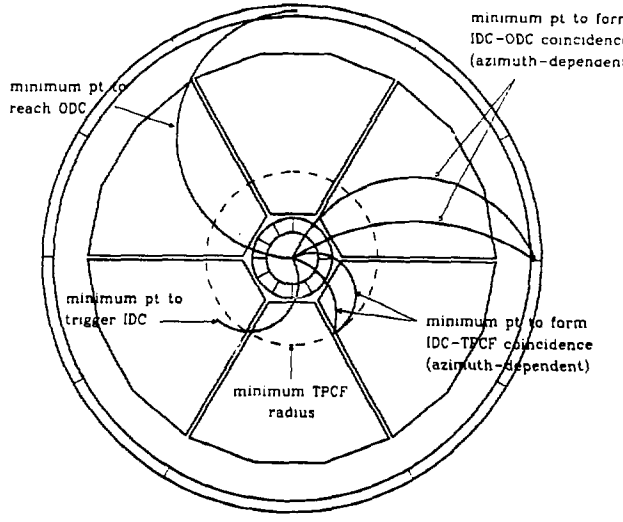

Figure 3.15: Tracks meeting different trigger minimum $p_\perp$ requirements.

3. *Maximum distance from the vertex.* Vertex requirements come from the timing of the trigger windows. Roughly, a track must approach within 10 to 20 cm of the interaction point.

4. *Restrictions on decays.* If a particle decays in the TPC volume, it will still be considered by the trigger as a single track. The decay, therefore, must be such that the two tracks combined satisfy the $p_\perp$ and vertex requirements above.

5. *Limited nuclear interactions.* Large angle tracks (with the angle measured from the beamline) must cross through the ODC to trigger. To do so they must pass through the IDC, TPC, and the .87 radiation length magnet coil between the TPC and the ODC. The loose angular coincidence required between TPC tracks and ODC hits allows some interactions, but not those with produce only particles at large angles, with no charge, or with very low energies. This restriction also makes the trigger probability species-dependent[38]: Figure 3.16 shows curves of the measured probability of an ODC hit as a function of $p_\perp$ and particle type. (An overall ODC inefficiency of 90% is included in this measurement.)

In addition to these requirements on individual tracks the trigger logic puts azimuth-dependent requirements on the angle between two tracks. Two tracks must be separated by 60° to 90° in azimuth because of the pre-pretrigger requirement of two intervening 30° IDC sections.

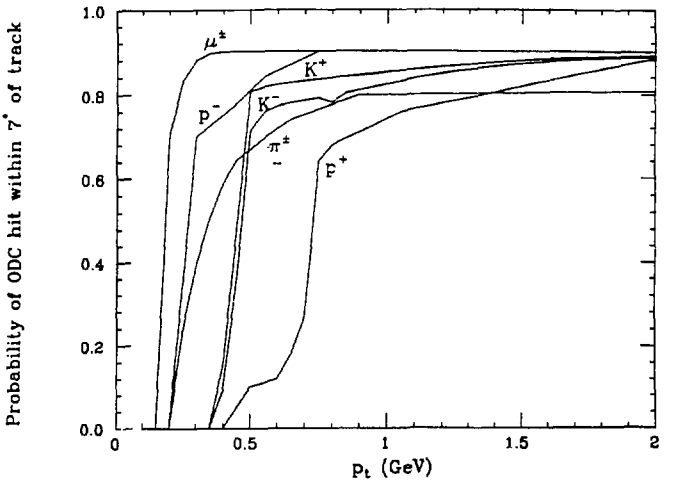

Figure 3.16: Measured probability of a hit in the ODC within 7° of the extrapolated track, as a function of particle type and charge. The angular coincidence required by the trigger is looser, but the probability of satisfying it is more difficult to measure.

Chapter 4

Data Processing and Simulation

4.1 Data Processing

The goal of data processing is to convert the information about each event from its detector-element oriented "raw" form to a track and photon oriented form. This procedure is also often referred to as "event reconstruction". Some of the results of data processing have already been given in the detector descriptions of the previous chapter. However, when considering heavy lepton searches it's useful also to have an overall view of the procedure, becuase it is the framework not only of the event reconstruction but of event selection. When planning any analysis method, but particularly one for an unanticipated project such as a new particle search, it's usually found that some information or events which could have been useful have been dropped in the course of the reconstruction. The stages at which the various event selection cuts (called filters) are applied determines how far back one has to go to pick up lost events, and if they are recoverable at all.

As it turned out, luckily most of the heavy lepton events were kept because they resemble interesting two-photon events. The results of Chapter 5 were little affected by the filters. The studies of Chapter 6 indicate, on the other hand, that changes in the filters and earlier stages of the processing might be helpful (but such changes have not yet been tried).

Data structure		*Num tapes*	*Num events*
real (physical) event			millions
Filter:	Trigger		
Processing:	readout of detector electronics		
LDB image / buffer			5,410,000
Filter:	Preanalysis		
Processing:	detector setup, Cluster, Pattern, Hawire		
raw data tape		1500	3,590,000
Filter:	TPC Select, Bhabha Count, Strip Cosmic		
Processing:	whatever wasn't finished of Cluster, Pattern, and Hawire then Distort (preliminary) + subsequent routines		
E tape		1030	1,770,000
Filter:	SelTwoGam		
Processing:	Distort (final) + subsequent routines, MakeDST		
F tape		327	835,000
DST tape		11	835,000

Table 4.1: Sequence of data processing events.

4.1.1 The Processing Chain

Table 4.1 gives the sequence of data handling events. After each beam crossing a trigger decision is made. If the trigger is satisfied the data stored by the detector electronics are transferred to a set of memory boards called the Large Data Buffer (LDB). Once the data are read into the LDB, the detector can be reset. Meanwhile the "LDB image" is read from the LDB into the online memory and there is then usually some time available to look at the data; it doesn't immediately have to be written to tape. During that time as many stages of data processing are run as there is time for. The first few stages, "Cluster", "Pattern" and "Hawire", are reconstruction routines which group TPC pad and wire hits into clusters, group the pad clusters into tracks, and assign wire clusters to the tracks. All this information, together with the raw data, is then stored on

tape.

The next stage of analysis is a first pass through the remainder of the data processing: looking at the information from other detector subsystems, and trying to fit and identify tracks. The results are written to a new set of "E" tapes.

The data events are divided into five groups called Experiments, during which running conditions and detector parameters are kept unchanged (as much as possible). When an Experiment is finished, the average properties of the track fits are checked and overall "distortion corrections" are determined from them. Then the analysis is rerun with these corrections, and selected events are written to two more sets of tapes: "F" tapes containing all available information on each event, and "Data Summary Tapes" (DST's) which contain for each event a list of tracks and photons, along with those of their properties which are considered most useful, and selected information about the event as a whole. Analyses designed to answer specific physics questions take over at this point, based on information from either the F tapes or the DST's.

4.1.2 Filters

The trigger is only the first of several filters applied to the data. All the filters are designed to remove unwanted events from the data while keeping all interesting events. Their purpose is to reduce the number of events which have to be handled in subsequent processing steps. Filters must be given special attention in a search for new particles because if the particles are not found, the result will be limits based on the absence of certain kinds of events. So it is necessary to be sure that such events would have been found had they been there. Also, filters are an acceptance correction which is normally ignored because they are designed to fail safely, keeping all possibly interesting events. Since the characteristics of new particle events may not have been anticipated, it can't be assumed that the

filters are safe for them as well.

In the TPC data processing, the filters are designed to remove the background described in Section 3.1. So they look for low multiplicity and/or low energy events to remove the two-photon QED events, and for non-vertex tracks to remove the non-e^+e^- background (cosmic rays and beam gas events). It turns out that heavy lepton events look much like the background the filters are trying to remove. They tend to be low multiplicity and to have low energy (because of the missing massive neutrinos), and if their lifetimes are long, the observed daughter particles will be non-vertex tracks. This means that, as with the trigger, an awareness of the filters is useful when deciding how to look for heavy leptons.

Preanalysis

Preanalysis is run while each event is stored in memory but before it is written to tape. For every "track" that the trigger logic found, preanalysis (described in detail in Reference [35]) checks that there is a pattern of pad and wire hits consistent with such a track. It is thus designed to be a trigger verification. Its basic premise is that any interesting (charged trigger) event will have at least two good vertex tracks. As long as the events being sought have two such tracks, it can be safely assumed that they will pass preanalysis: it has been checked that it doesn't reject good events.

For other kinds of events (those for example with non-vertex tracks or kinked tracks) it's difficult to tell, from a description of how it works, what preanalysis will do. Therefore, its effect as a filter must either be avoided by requiring two good vertex tracks as part of the event selection, or completely accounted for by running preanalysis on simulated events.

TPC Select

As soon as tracks have been found and fitted with trajectories by Pattern, and before any further analysis is done, another set of filters is used to reject more unwanted events. These three filters are called TPC Select, Strip Cosmic, and Count Bhabha. Only events passing the filters are written to the next set of tapes (E tapes). The second and third filters have little effect on heavy lepton events: Strip Cosmic removes events which leave a track in the muon chambers but miss the TPC, while Count Bhabha removes 80% of the events identified by the poletip calorimeter as Bhabhas. TPC Select, however, tightens the vertex cuts applied to low multiplicity events, and so must be taken into consideration. An event can pass TPC Select only in one of the following ways:

1. If there are three or more good tracks, or two or more calorimeter hits, the event is always accepted.

2. If there are no calorimeter hits, then there must be either:

   (a) exactly one good track, and no bad tracks, or

   (b) exactly two good tracks (any number of bad tracks), and either their colinearity angle is less than 176 degrees or one comes within 2.5 cm of the beamline.

3. If there is one calorimeter hit, there must be either

   (a) at least one good track, or

   (b) no tracks (good or bad).

In these definitions, a good track is one which comes within 5 cm of the beamline and 10 cm from the midplane at the point of its closest approach to the beamline. The definition of calorimeter hits is more complicated but requires at least 750 MeV in at least one calorimeter module.

For two-track events with no calorimeter hits (typical of heavy lepton events), TPC Select can be summarized as requiring that both tracks must come fairly close to the vertex, and if the tracks are colinear that one track must come very close to the vertex.

SelTwoGam

SelTwoGam (standing for Select Two Gamma) is the filter between the E tapes and the F tapes. It selects $q\bar{q}$, $\tau^+\tau^-$, and some two-photon events. About 40% of E tape events pass SelTwoGam. SelTwoGam makes decisions based on both charged and neutral information, and has been described in Reference [39]. As with the trigger, because heavy lepton events usually only have charged visible energy, only the charged SelTwoGam selection is considered here.

The charged selection first classifies events according to the number of "prongs": tracks which pass the vertex cuts $x < 7.5$ cm, $y < 7.5$ cm, $z < 25$ cm at the closest approach of the track to the beam, and which have $p_\perp > 150$ MeV. Events with fewer than two prongs are rejected, while those with three or more prongs are accepted.

If the event has exactly two prongs it is classified as colinear if the angle between the two prongs is greater than 160° and the total charged energy of the event is greater than 8 GeV. If it is colinear it is accepted only if the two prongs were fit to a common vertex during data processing.

If the event is not colinear it is placed in one of the following four classes:

1. K or p event: either track has $\chi^2_K < 10$ or $\chi^2_p < 10$,
2. μ or π event: either track has $\chi^2_\mu < 10$ or $\chi^2_\pi < 10$, and neither has $\chi^2_K < 10$ or $\chi^2_p < 10$,
3. $2e$ event: both tracks have $\chi^2_e < 10$, and neither has $\chi^2_\mu, \chi^2_\pi, \chi^2_K or \chi^2_p < 10$,

4. All other events.

Events from classes 1 and 4 are always accepted. Class 2 and 3 events are accepted if the square of their invariant mass is greater than 1.5 GeV^2. Class 2 events are also accepted if their coplanarity angle is less than 170°. If an event is accepted by charged SelTwoGam selection, it will pass all of SelTwoGam unless it also appears as a Bhabha event in the Poletip calorimeter, or (for half the data) in the Hex calorimeter. Bhabhas are rejected.

SelTwoGam may by summarized as rejecting low-mass e^+e^- events, low-mass coplanar $\mu^+\mu^-$ and $\pi^+\pi^-$ events, Bhabha e^+e^- events, and cosmic rays, but keeping any events which have a chance of being anything else. In the searches for heavy leptons, both data and simulated events where always required to pass the charged SelTwoGam cuts given above. Data events which passed the neutral but not the charged selection were not considered.

4.2 Monte Carlo Simulations

Monte Carlo simulations are used in high energy physics experiments both to check the performance of the analysis programs, and to predict the results of physical processes as they will appear in the detector. They begin with the well-defined but probabilistic physics rules which particles must obey and follow the rules to generate random events. The average properties of the events are therefore determined by these rules, and may be used to check them by comparing Monte Carlo simulated events with real events. For simple problems such expected distributions can be found analytically, but Monte Carlo is usually the most practical way of making predictions about high energy physics events, which are complicated by the sequential application of large numbers of rules governing both the creation of particles and their interactions with the detector.

Descriptions of the use of Monte Carlo in the heavy lepton analyses are in-

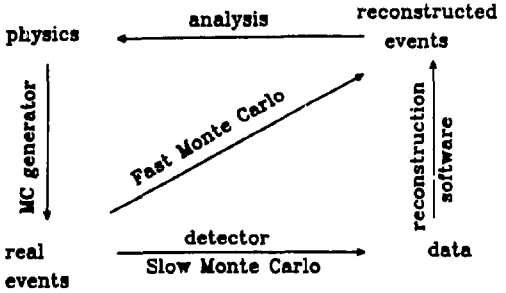

Figure 4.1: Schematic diagram of the relationship between real and simulated events and event reconstruction.

cluded in the descriptions of the searches given in the next two chapters. This section provides a general picture of what simulations are available and of some of their properties.

Figure 4.1 is a diagram of the steps involved in getting the answer to a physics question from our experiment. The Fast Monte Carlo simulates reconstructed events directly from generated events, by using wherever possible parametrizations which reflect the available understanding of the behavior of the detector and of the processing software. The Slow Monte Carlo, on the other hand, assumes as little as possible about the detector and nothing about the analysis software, relying mostly on basic physics and geometry. For the TPC these two simulations are called the FMC (Fast Monte Carlo) and GLOBAL.

The standard version of the FMC simulates only the tracking part of the detector (the TPC), since this is the best understood and the most heavily used in analysis. (Other detector simulations are sometimes added as needed for specific analysis problems, but are usually not checked out carefully enough to be reliable for other problems.) The FMC results are lists of reconstucted tracks

and photons, and are given in the DST format (the end product of the analysis chain of Table 4.1).

Because none of the information at intermediate stages of processing is simulated, none of the software filters of the previous section can be applied directly to FMC events. Instead their effects must be studied and approximated (in keeping with the general philosophy of a fast Monte Carlo).

Low multiplicity simulated events must also be corrected for trigger acceptance and efficiency. The behavior of the trigger for such events, however, is highly dependent on the details of the event and so is difficult to approximate. The "Fast Trigger Monte Carlo"[40] which is used with FMC events is therefore in philosophy partly a slow simulation: it begins with the DST list of tracks, simulates the detector hits they would have produced, and applies the actual trigger logic to these hits. Some approximations are made: one is beginning with the list of tracks found, rather than the list of tracks generated. Others include parametrizations of the probability of particles getting through the materials in the detector, and of the drift chamber efficiencies.

The Slow Monte Carlo, GLOBAL, takes the generated list of charged and neutral particles and tracks them all the way through all the detectors. GLOBAL results are a list of detector hits in the "raw data" format as it is first written to tape. The effects of analysis filters and data processing can then be exactly determined for each event. The trigger decision is simulated with the same software as is used in the FMC, only in this case the information about detector hits is supplied to it by the GLOBAL simulation rather than specifically generated for the trigger. (The most difficult problem with using GLOBAL is keeping track of the parameters in the processing which are tuned to the data, and making sure that they are properly set for simulated GLOBAL data.)

Monte Carlo simulations are only a useful analysis tool if their accuracy is

known and reliable. For the search described in Chapter 5, the FMC was used in ways which have been previously used and checked by other analyses. In addition, data and Monte Carlo predictions of $\tau^+\tau^-$ events were found to agree well. A test measurement of $\mu^+\mu^-$ cross sections (not described here) was also in good agreement with the FMC. So the systematic errors from the Monte Carlo simulations were judged to be small. For the searches studied in Chapter 6, however, the Monte Carlos were used in less standard ways and the predictions were felt to be correspondingly less reliable (though not necessarily less accurate). The lack of checks of these applications is the principal reason that the analyses described in Chapter 6 are classed as studies and not results.

Chapter 5

The Search for New Leptons

A search for a new particle can be unsuccessful for one of two reasons: either because the particle doesn't exist, or because the signals it produces are undetectable. Whether or not a signal is detectable depends in turn on the physics involved, on the properties of the detector, on the software used to analyze the data it collects, and on the accumulated understanding of the properties of all three. Some of these ingredients have been discussed in the preceding chapters. Based on them, four methods of searching for heavy leptons with the TPC were devised. The first method, described in this chapter, turned out to be a good search technique for all heavy leptons with $\Delta m > .3$ to .4 GeV (and $m_L < 12$ GeV). The other three methods were designed to search the remaining low-Δm region, and are explained in Chapter 6.

5.1 $e - \pi/\mu$ Search

The first search was for L^+L^- pairs decaying through

$$L^- \rightarrow e^-\overline{\nu}_e\nu_L,\ L^+ \rightarrow \mu^+\nu_\mu\overline{\nu}_L \text{ or } \pi^+\overline{\nu}_L + (\geq 0 \text{ neutral hadrons})$$

(or the charge conjugate decays). The search therefore was for events with exactly two tracks, one an electron and the other a pion or muon of the opposite sign. The advantage of the searching for an $e - \pi/\mu$ signal is that the TPC's good

particle identification can then be used to avoid the large e^+e^-, $\mu^+\mu^-$, and $\pi^+\pi^-$ backgrounds from QED and two-photon processes. A second advantage is that both decay modes are relatively common whenever Δm is less than 2 to 3 GeV, so this signature can be used to search for heavy leptons over most of the m_L,Δm space open to them.

5.2 Event Selection

The $e - \pi/\mu$ event sample was defined by requiring all events to pass the following cuts:

1. There were exactly two tracks, both good, one an unambiguous electron and the other consistent with a pion and not consistent with an electron. These were defined as:

   (a) good track

      i. The distance r of the track from the beamline at its closest approach to the beamline was less than 6 cm.

      ii. The distance z of the track from the midplane at its closest approach to the beamline was less than 10 cm.

      iii. The transverse momentum $p_\perp$ of each track was greater than 150 MeV.

      iv. The curvature error $dC = (dp_\perp/p_\perp^2)$ satisfied $dC < .3\text{GeV}^{-1}$ and $p_\perp dC < .3$.

   (b) unambiguous electron

      i. The dE/dx particle identification gave $\chi_e^2 < 4$, $\chi_e^2 + 4 < \chi_\mu^2$ and χ_π^2, and $\chi_e^2 + 8 < \chi_K^2$ and χ_p^2, and there were more than 40 dE/dx measurements along the track.

      ii. The momentum was between 0.3 GeV and 15 GeV.

iii. The track was not identified as a muon by the muon chambers.

iv. The track was not part of a reconstructed photon conversion pair.

(c) consistent pion (and inconsistent electron)

i. The dE/dx particle identification gave $\chi^2_\pi < 4$, $\chi^2_\pi + 8 < \chi^2_e$, and $\chi^2_e - 5 < \chi^2_\mu$ and χ^2_K and χ^2_p, and and there were more than 40 dE/dx measurements along the track.

ii. The momentum was less than 8 GeV.

2. The colinearity angle (the angle between the two tracks) was less than 177°.

3. The coplanarity angle (the angle between the two tracks when projected into the plane perpendicular to the beamline) was less than 178°.

4. Either the coplanarity angle was less than 170°, or M^2, the square of the invariant mass of the two tracks, was greater than 1.5 GeV^2, where $M^2 = 2p_1p_2(1 - \cos\theta_{colinearity})$ (with the particle masses neglected).

5. The averaged z-position of the two tracks at their closest approach to the beam, $(z_1 + z_2)/2$, was less than 4 cm from z_{beam}, the average interaction point.

6. The tracks were of opposite sign. (Same-sign events were also kept as a separate sample.)

7. The ripple trigger was satisfied.

8. The charged SelTwoGam cuts were satisfied.

There were 587 opposite-sign events which passed all cuts and 200 same-sign events. Figure 5.1 shows the dE/dx vs $\ln p$ distributions of the electron candidates in "$x - \pi/\mu$" events (a) before and (b) after electron dE/dx cuts. The π/μ track not shown was in both cases identified by pion dE/dx cuts. The few

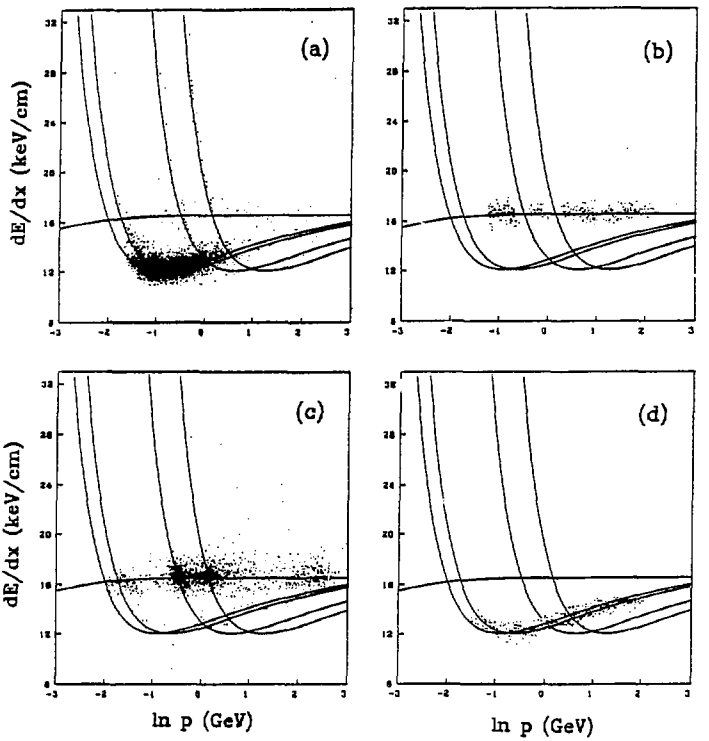

Figure 5.1: The dE/dx vs $\ln p$ distributions of (a) candidate electrons in $x - \pi/\mu$ events before the electron dE/dx χ^2 cuts, and (b) those which pass the χ^2 cuts. Plots (c) and (d) show the analogous distributions for pion candidates and accepted pions in $e - x$ events. (In (a) and (c) only one tenth of the data is shown.)

$e-\pi/\mu$ events are clearly separated from the many $\pi^+\pi^-$ and $\mu^+\mu^-$ events in most of the momentum range. Figures 5.1(c) and (d) show the corresponding plots for pion candidates in "$e-x$" events.

5.3 Monte Carlo Corrections

There were four major sources of events which the cuts were not designed to discriminate against. These were: $e^+e^- \rightarrow L^+L^-$, $e^+e^- \rightarrow \tau^+\tau^-$, $e^+e^- \rightarrow e^+e^-\tau^+\tau^-$, and events with more than two tracks but with only two found.

No cuts were made against the two kinds of tau events because they are too similar to heavy lepton events. The annihilation tau events *are* heavy lepton events, so a cut against them would remove the region around $m_L = m_\tau$, $\Delta m = m_\tau$ from the m_L,Δm region which could be searched, and reduce the number of events from other regions. The two-photon tau events, because they produce low-energy rather than beam-energy τ's, are even less distinguishable from L^+L^- events. So instead of cuts, Monte Carlo simulations of annihilation and two-photon tau pair production were used to find out how many of the data events came from these two sources. The contribution of the fourth source of $e-\pi/\mu$ events, those with missing tracks, was estimated directly from the data, not from Monte Carlo, so the analysis used just three sets of simulated events: $\tau^+\tau^-$, $e^+e^-\tau^+\tau^-$, and L^+L^-(of which there were many subsets).

An advantage of using Monte Carlo to correct for the tau events instead of making cuts against them was that it was also an opportunity to check the $\tau^+\tau^-$ Monte Carlo. The cuts were, in fact, designed to keep as many $e^+e^- \rightarrow \tau^+\tau^-$ events as possible, so that the Monte Carlo could be compared with the data in regions of phase space where heavy lepton events weren't expected. This was an important check because the same $e^+e^- \rightarrow \tau^+\tau^-$ Monte Carlo, with only parameters changed, was then used to find what events would be expected from

production of heavy leptons. Good agreement between the $\tau^+\tau^-$ Monte Carlo and the data made it unlikely that there were major systematic errors in the heavy lepton Monte Carlo.

An advantage of using Monte Carlo *only* to correct for $\tau^+\tau^-$ and $e^+e^-\tau^+\tau^-$ events is that these come from QED and therefore well-understood processes (and the branching ratios of τ decays are also fairly well-measured). The confidence placed in this understanding is such that Monte Carlo corrections for $e^+e^-\tau^+\tau^-$events are routinely made although the cross section has in fact never been explicitly measured.

For all the simulations, the Fast Monte Carlo (FMC) was used, both because large numbers of L^+L^- events were needed (to survey the whole range of m_L, Δm values), and because the FMC detector simulation has the best-tuned handling of TPC particle identification, on which the event selection relies heavily. Two different event generators were used. The two-photon tau events were generated by the Vermaseren Monte Carlo, which uses an exact QED calculation to find the distributions from which the events are drawn[41,42,43,32]. The events include both the $\tau^+\tau^-$ pair and the scattered electron and positron. The 33,000 $e^+e^-\tau^+\tau^-$ events used were actually the same events that have been used to correct for background from tau production in TPC two-photon studies, although the detector simulations used with them were different. The event generator for the annihilation events was a version of the Berends and Kleiss $\mu^+\mu^-$ generator[44] which has been adapted to $\tau^+\tau^-$ events and simplified in its handling of final state radiation. This generator has also been used for several previous TPC/2γ studies.

For the heavy lepton simulation, the $\tau^+\tau^-$generator was again used, with specified values for m_L and m_{ν_L}, while special lifetime and branching ratio tables were added to the detector simulation. (In both cases, a new fourth lepton was

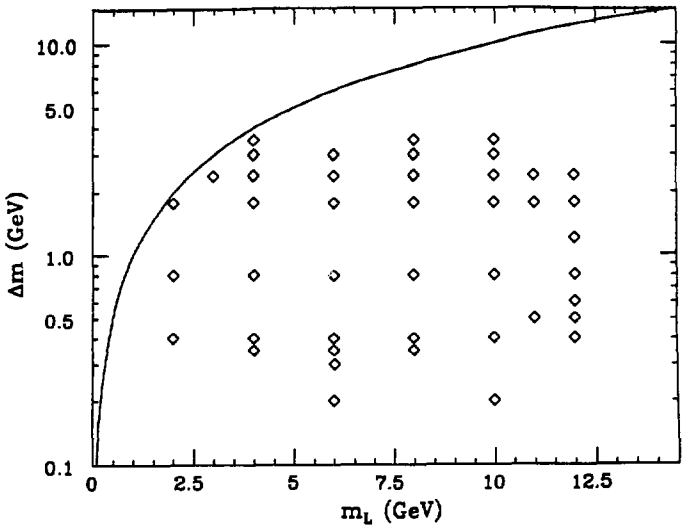

Figure 5.2: Combinations of m_L and Δm for which Monte Carlo events were generated.

generated, so that the τ was still available as a possible decay product and as a small radiative correction.) This heavy lepton Monte Carlo was then used to generate 20,000 L^+L^- events at each of 43 m_L,Δm points. Figure 5.2 shows their distribution in a m_L,Δm plot. A grid of evenly spaced points was used first to find roughly where the search method would be effective, and then a second set of points was concentrated along the edges of that region.

5.4 Missing-track Background

As stated above, the three known sources of $e - \pi/\mu$ events are $\tau^+\tau^-$, $e^+e^-\tau^+\tau^-$, and missing-track events. Losing one or more tracks, however, removes most of the charge correlation between the two remaining tracks, particularly if they

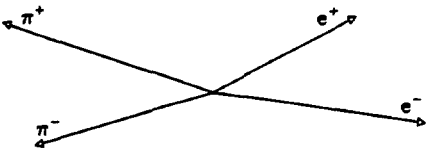

Possible 2–track	$\pi^+ \pi^-$	$\pi^+ e^+$	$\pi^+ e^-$
combinations :	$e^+ e^-$	$\pi^- e^-$	$\pi^- e^+$

Figure 5.3: Six ways of finding only two out of four tracks: if only unlike particles are accepted, there are two opposite-sign pairs and two same-sign pairs.

are of different particle types. This is demonstrated for a simple case in Figure 5.3. Therefore, the numbers of opposite-sign and same-sign missing-track events will be equal, and their contribution can be removed from any histogram of the opposite-sign $e - \pi/\mu$ sample by subtracting the corresponding histogram of same-sign events.

This correction will not work properly if there are any processes which produce same-sign $e - \pi/\mu$ pairs preferentially. We could not think of any such process, but have no proof that there are none. On the other hand, there are several ways in which opposite-sign pairs are produced preferentially, for example, by misidentification of either particle of a e^+e^-, $\mu^+\mu^-$ or $\pi^+\pi^-$ pair, by $\mu^+\mu^-$ events in which one of the muons decays to an electron (these occur despite the long muon lifetime because there are so many two-photon $\mu^+\mu^-$ events), and by the tendency of all events to conserve charge. For setting limits, therefore, subtraction of same-sign events is believed to be a conservative correction. This assumption is strengthened by the observation that in all the distributions studied this correction never gave statistically significant negative numbers of events

in any histogram bin.

5.5 Comparison of Distributions, Limits

An example of the comparison between heavy lepton predictions and data is given in Figure 5.4; in this example $m_L = 8$ GeV, $\Delta m = 0.8$ GeV. The data points in each distribution are from events which pass all cuts, and have also been corrected as described in the previous two sections. Thus in each bin i:

$$\begin{aligned} n_{i,\text{data}} &= (n_{i,\text{data,opposite-sign}} - n_{i,\text{data,same-sign}}) \\ &- (n_{i,\tau^+\tau^-,\text{opposite-sign}} - n_{i,\tau^+\tau^-,\text{same-sign}}) \times \text{scale-factor}_{\tau^+\tau^-} \\ &- (n_{i,e^+e^-\tau^+\tau^-,\text{opposite-sign}} - n_{i,e^+e^-\tau^+\tau^-,\text{same-sign}}) \times \text{scale-factor}_{e^+e^-\tau^+\tau^-}, \end{aligned}$$

where the scale factor = Luminosity × cross section / number of Monte Carlo events. Figures 5.5 and 5.6 show how this correction works for a histogram of electron momentum. The heavy lepton histograms are also scaled to be directly comparable to the data (making the assumption that the cross section for $e^+e^- \to L^+L^-$ can be calculated in the same way as for the light leptons). So,

$$n_{i,L^+L^-} = (n_{i,L^+L^-,\text{opposite-sign}} - n_{i,L^+L^-,\text{same-sign}}) \times \text{scale-factor}_{L^+L^-} \ .$$

Just by inspection, it is clear from several of the histograms in this example that the data are incompatible with the production of heavy leptons at the point $m_L = 8$ GeV, $\Delta m = 0.8$ GeV.

To define a region in which heavy leptons are excluded, heavy lepton (Monte Carlo) histograms of the momentum of the electron in each event are compared with the data at the 43 points for which Monte Carlo events were generated. The distributions of several variables show large differences between the data and heavy lepton predictions; of these, the p_e distribution was chosen for limit-setting because its variation with m_L and Δm is simple: p_e is less when there is less energy available for the decay (Δm is small), or when the Lorentz boost of

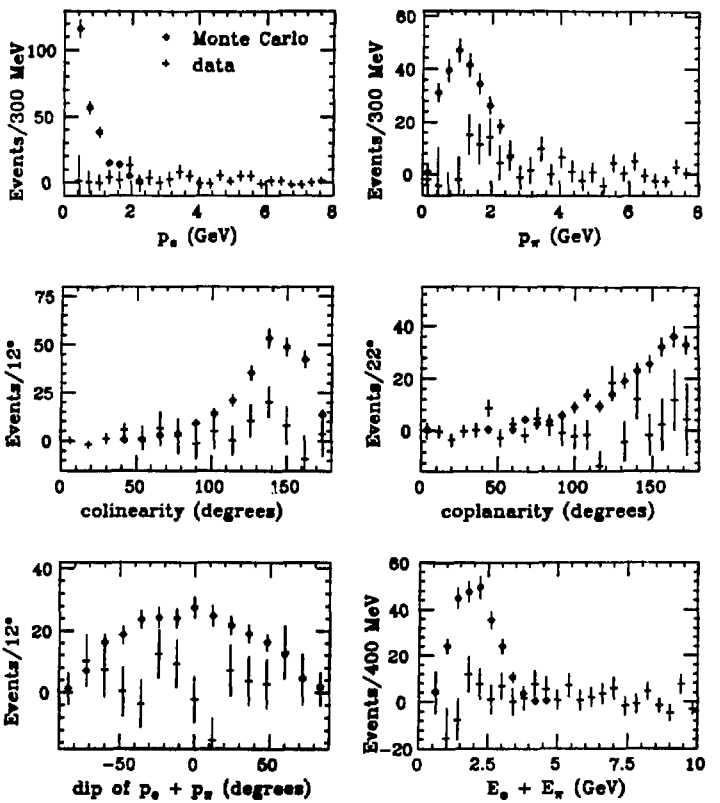

Figure 5.4: Distributions of six variables from data events and from Monte Carlo events with $m_L = 8$ GeV, $\Delta m = 0.8$ GeV. The number of Monte Carlo events is scaled so that the pairs of histograms can be directly compared.

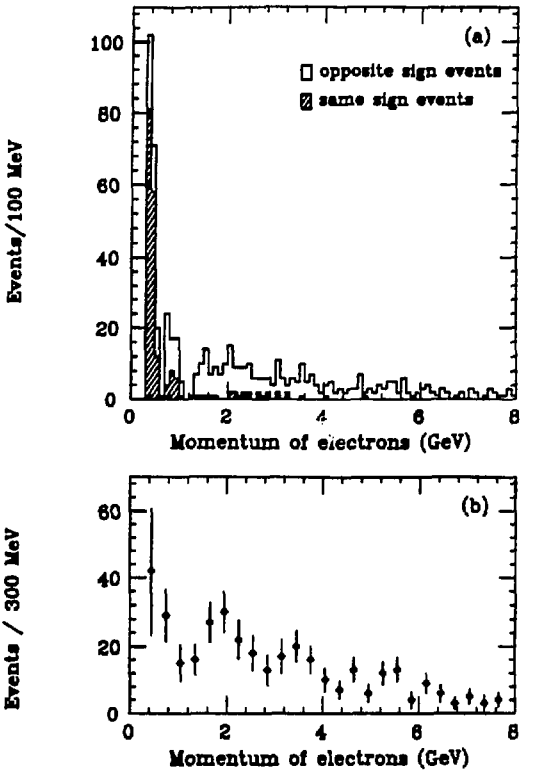

Figure 5.5: (a) Momentum distribution of the electrons in same-sign and opposite-sign data events. (b) The difference between the number of opposite-sign and same-sign events, as a function of electron momentum.

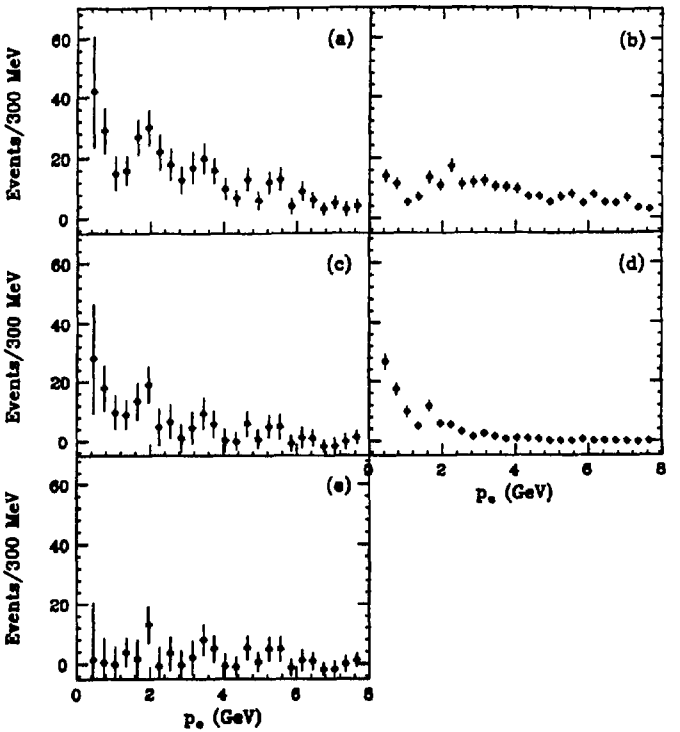

Figure 5.6: Distributions of electron momentum for (a) data (the same as Figure 5.5(b)), (b) Monte Carlo for $e^+e^- \to \tau^+\tau^-$, (c) data with the annihilation $\tau^+\tau^-$ contribution subtracted, (d) Monte Carlo for $e^+e^- \to e^+e^-\tau^+\tau^-$, and (e) data with annihilation and two-photon $\tau^+\tau^-$ contributions subtracted.

the decay center of mass is small (m_L is large). So it can be assumed that the p_e distributions change smoothly with Δm and m_L, and that there are no small regions of heavy lepton compatibility in between the grid points in the excluded region.

To quantify the comparison between data and heavy lepton Monte Carlo, for each of the heavy lepton points a maximum bin number $i_{80\%}$ is chosen such that $\sum_{i=1}^{i_{80\%}} n_{i,L^+L^-} \geq 0.8 \times \sum_{allbins} n_{i,L^+L^-}$. A chi-squared is then defined by

$$\chi^2 = \frac{(N_{L^+L^-} - N_{data})^2}{\sigma^2_{L^+L^-} + \sigma^2_{data}}$$

where $N_{L^+L^-} = \sum_{i=1}^{i_{80\%}} n_{i,L^+L^-}$, $N_{data} = \sum_{i=1}^{i_{80\%}} n_{i,data}$, $\sigma^2_{L^+L^-} = \sum_{i=1}^{i_{80\%}} \sigma^2_{i,L^+L^-}$, and $\sigma^2_{data} = \sum_{i=1}^{i_{80\%}} \sigma^2_{i,data}$. The confidence level is then $(1/\sqrt{2\pi}) \int_{-\infty}^{\chi} e^{-x^2/2} dx$, and is greater than 99% for $\chi > 2.33$. In the example of Figure 5.4, $\chi^2 = 60$ and the confidence level is $\gg 99\%$. (In the calculation of χ^2, histograms with 100 MeV bins are used, so this exact χ^2 can't be obtained directly from Figure 5.4.) The choice of 80% is arbitrary; 70% or 90% give essentially the same answers. It is clear that this is a straightforward rather than a sophisticated statistical method.

With this definition of the confidence level, and with statistical errors only, heavy leptons with m_L,Δm values within the dashed line of Figure 5.7 are excluded at the 99% confidence level.

5.6 Systematic Errors

The main sources of systematic error are listed below, roughly in order of decreasing importance.

1. *Luminosity.* Since both the tau corrections and the heavy lepton predictions are scaled by the luminosity, an error in luminosity has a double effect: if the true luminosity is less than the measured value, more of the data is

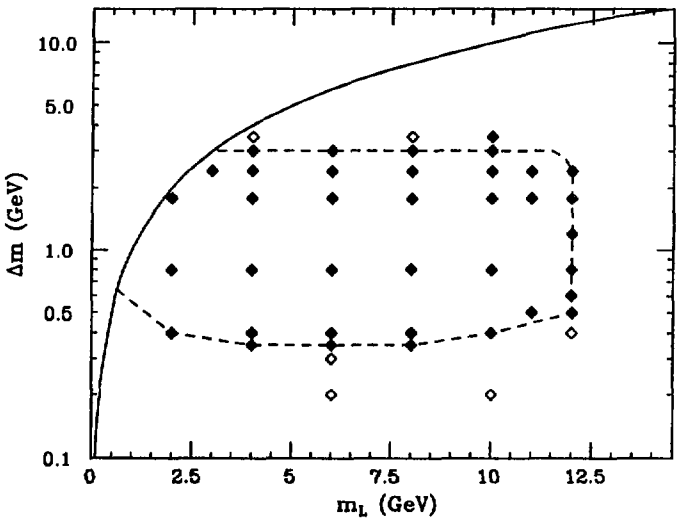

Figure 5.7: Region of m_L,Δm excluded at the 99% confidence level, with statistical errors only.

unaccounted for, and fewer heavy lepton events are expected. The error in the luminosity is 10%[45]; the fourth column of Table 5.1 gives χ if the Monte Carlo scale factors are all reduced by 10%.

2. *Trigger efficiency.* The trigger acceptance corrections given by the trigger simulation are also believed to be accurate to about 10%, at least in the case of the ripple trigger, which has been the most carefully studied. As a check that this accuracy holds specifically for $e - \pi/\mu$ events, a second data sample was defined by changing the event selection cuts to require a calorimeter trigger rather than a ripple trigger. The trigger simulation was applied to these events and the predicted and actual fraction of events with ripple triggers (in addition to the calorimeter trigger) were compared. The results are given in Table 5.2, and are consistent with 10% accuracy. A 10% overestimate of the trigger efficiency, although it would probably be somewhat momentum and topology dependent, would have approximately the same effect as a 10% overestimate of the luminosity, so the effects on χ are also given by Column 4 of Table 5.1.

3. *Decay correlations.* As described in Section 2.4, the electrons and pions from heavy lepton decays have somewhat correlated momenta because of the correlated helicities of the parents. The correlations are of the form $(1 + \alpha_e \cos\theta_e)$ and $(1 + \alpha_\pi \cos\theta_\pi)$, where θ is the angle of the decay of the heavy lepton relative to its spin, in its rest frame, and the maximum

Δm	m_L	no sys err	90% Lum	no $2\gamma\ \tau^+\tau^-$	90% s-s	85% Lum	C.L.
.2	6	0.81	0.55	0.40	0.04	0.41	.66
	10	0.34	0.46	1.10	0.97	0.52	.70
.3	6	2.33	1.81	0.65	1.62	1.54	.94
.35	4	5.43	4.58	3.15	4.82	4.14	>.99
	6	3.56	2.93	1.90	2.90	2.61	>.99
	8	2.85	2.36	1.49	2.15	2.12	.98
.4	2	7.07	5.79	4.00	6.53	5.13	>.99
	4	6.41	5.45	4.04	5.84	4.96	>.99
	6	6.07	5.21	4.09	5.50	4.77	>.99
	8	3.90	3.32	2.54	3.24	3.02	>.99
	10	2.81	2.36	1.64	2.14	2.14	.98
	12	1.18	0.87	0.03	0.42	0.72	.76
.5	11	3.66	3.10	2.31	3.00	2.82	>.99
	12	2.96	2.50	1.79	2.30	2.26	.99
.6	12	4.27	3.66	2.93	3.63	3.35	>.99
.8	2	7.49	5.95	4.37	6.97	5.15	>.99
	4	8.72	7.31	5.68	8.23	6.58	>.99
	6	8.15	6.94	5.40	7.64	6.32	>.99
	8	7.72	6.69	5.50	7.20	6.16	>.99
	10	6.17	5.28	4.16	5.59	4.83	>.99
	12	4.50	3.90	3.19	3.89	3.59	>.99
1.2	12	5.77	4.87	3.45	5.16	4.41	>.99
1.784	2	5.98	4.41	2.83	5.43	3.60	>.99
	4	8.87	7.21	5.78	8.38	6.34	>.99
	6	8.93	7.42	5.84	8.44	6.64	>.99
	8	8.04	6.62	4.89	7.53	5.88	>.99
	10	6.97	5.79	4.01	6.42	5.19	>.99
	11	6.26	5.16	3.32	5.69	4.59	>.99
	12	4.55	3.64	1.73	3.93	3.17	>.99
2.4	3	3.99	2.58	0.73	3.38	1.87	.97
	4	4.83	3.39	1.57	4.24	2.66	>.99
	6	5.19	3.79	1.96	4.60	3.08	>.99
	8	5.71	4.43	2.48	5.13	3.78	>.99
	10	4.78	3.63	1.55	4.17	3.05	>.99
	11	3.91	2.87	0.69	3.27	2.34	.99
	12	3.02	2.08	0.18	2.35	1.59	.94
3.0	4	3.00	1.68	0.30	2.36	1.01	.84
	6	3.38	2.08	0.07	2.74	1.42	.92
	8	3.80	2.57	0.48	3.16	1.94	.97
	10	3.20	2.10	0.14	2.53	1.54	.94
3.5	4	2.15	0.88	1.17	1.49	0.23	.95
	8	2.15	0.9[illegible]	1.20	1.48	0.38	.65
	10	2.55	1.44	0.84	1.86	0.88	.81

Table 5.1: Values of χ with various systematic errors included

Category	Number of events
Ripple trigger set in data or Monte Carlo:	305
Ripple trigger set in data:	239 $(78.4 \pm 5.1\%)$
Ripple trigger set in Monte Carlo:	255 $(83.6 \pm 5.2\%)$

Table 5.2: Comparison of real and simulated ripple trigger efficiencies.

value of α_e and α_π is ± 1. If the L^+L^- spins are perfectly correlated the acceptance would by reduced for events at low Δm by at most a factor of $(1+ .25\alpha_e\alpha_\pi)$. Since $\alpha_e < .2$ for low Δm, the effect of angular correlations is to reduce the number of expected events by no more than 5%.

4. *Subtraction of tau backgrounds.* The branching ratios of tau decays are measured well enough that the uncertainty in the probability of events from $e - \pi/\mu$ decay is small: about 3%. So the error in this correction is dominated by the luminosity uncertainty considered above. The error in the subtraction of the $e^+e^-\tau^+\tau^-$background is more difficult to estimate, since there is no measurement of this cross section. To get an upper bound on the error, the analysis was redone without the two-photon $\tau^+\tau^-$correction. The resulting χ values are given in the fifth column of Table 5.1. If instead the reasonable assumption is made that the $e^+e^- \rightarrow e^+e^-\tau^+\tau^-$ predictions are right, then the error in this correction is probably also dominated by the luminosity uncertainty.

5. *Subtraction of same-sign events.* If there is an unknown source of same-sign events, the limits will be too strong. Column 6 of Table 5.1 gives the χ values if only 90% of the same-sign events are subtracted. In the absence

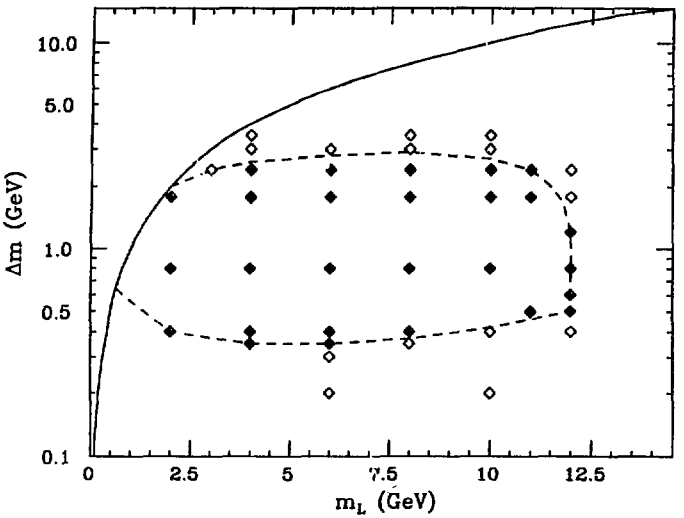

Figure 5.8: Region of m_L,Δm excluded at the 99% confidence level, with both statistical and systematic errors included.

of any reason to believe that the same-sign correction is wrong, however, and because the same-sign correction is itself a conservative correction, this effect is not included in the systematic error.

The total systematic error is estimated by scaling all the Monte Carlo corrections down by .85 (from $.85 = 1 - \sqrt{(.10_{luminosity})^2 + (.10_{trigger})^2 + (.03_{\tau^+\tau^-})^2}$). The results are the χ values and confidence levels in Columns 7 and 8 of Table 5.1. The effect of the systematic errors is to lower the confidence level for the excluded region of Figure 5.7 from 99% to about 90–95% along its upper edge, and 98% along its lower edge. Figure 5.8 shows the region excluded at the 99% confidence level when systematic errors are included.

Chapter 6

A Study of Searches at Small Δm

This chapter describes the results of a study of ways to look for leptons at $\Delta m < 400$ MeV. It was designed to answer the question "can we find leptons at small Δm with the TPC?" Three searches were tried; they and their results are described in Section 6.2. Although the study indicates that heavy leptons may be excluded in some new regions of m_L-Δm space, the systematics of the analyses have not been carefully studied (for reasons explained in Section 6.3), so these are not to be considered new limits. This chapter is included because the information may be helpful in the design of future searches.

6.1 A Description of the Problems at Small Δm

When the charged leptons and the associated neutrinos are very close in mass ($\Delta m < 400$ MeV), the events are different enough from those considered in the preceding chapter that new search methods are needed. The two characteristics of low Δm events are that the heavy leptons may have significant mean flight distances, and that their daughters often have energies below the threshold of the charged trigger. A third difference is that at low Δm the mean flight distances and the energies depend strongly on both m_L and Δm, so that search methods tend to be useful only in a limited m_L,Δm region.

The long lifetimes are a problem mostly because decays away from the vertex

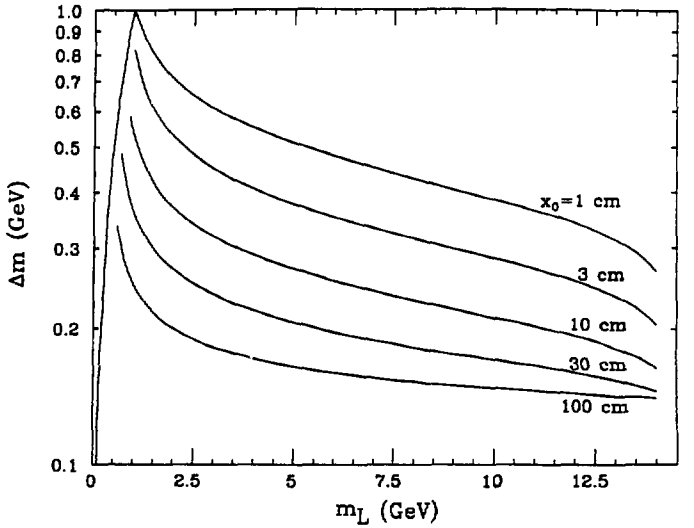

Figure 6.1: Contours of constant mean flight distance for heavy leptons with 14.5 GeV energy.

produce "non-vertex" tracks. Since the analysis filters generally require at least two vertex tracks, such decays cause the events to be rejected. (The various vertex requirements are given in Section 4.1.2; roughly, the track must extrapolate to within 5 cm of the beamline and 10 cm from the midplane.) In addition, if the mean flight distance is very large, then for some fraction of the events at least part of the detector will see the heavy lepton instead of its daughters. This, of course, can be turned from a problem into an advantage, but must be taken into account. Figure 6.1 shows contours of constant mean flight distance, x_0, in the m_L,Δm plane. These contours are correct for heavy leptons with PEP's 14.5 GeV beam energy. (Contours of constant mean life are independent of energy and approximately horizontal.) As x_0 varies from 3 cm to 100 cm, the topology of

the typical heavy lepton event changes dramatically. In Figure 6.2, five classes of topologies are shown schematically. To estimate what their relative probabilites are for a given x_0, three classes of decays are defined:

vertex	$x < 5$ cm	a decay near the beamline
TPC	50 cm $< x <$ 100 cm	a decay in the TPC volume, possibly reconstructable
outside	150 cm $< x$	a decay outside the Outer Drift Chamber; both TPC and trigger see the heavy lepton.

The probability of a particular decay type i is just $P_i = (e^{-x_{min,i}/x_0} - e^{-x_{max,i}/x_0})$, and the joint probability for an L^+L^- event to have two particular decay types i and j is $P_{ij} = 2 \times P_i \times P_j$, where the factor of 2 allows for the two ways of pairing the heavy lepton charges with the decay types. Some single (decay type) and joint (event type) probabilities are plotted in Figure 6.3. They serve as a guide to choosing the best way to look for a lepton of a given x_0. For example, two vertex tracks is the most likely topology for $x_0 < 30$ cm. However, detection also depends on background, and on event selection efficiencies which vary with Δm, with m_L, and with the topology type. These variables are considered in connection with specific searches in the next section.

The other problem with low Δm events is the low trigger efficiency for low energy tracks, which comes from the minimum transverse momentum requirements discussed in Section 3.3.2. If both heavy leptons decay to $\pi\nu_L$, Figure 6.4 shows contours of probability that both pions in the event have transverse momentum over 350 MeV, the approximate trigger threshold. Including pion-pion decay correlations would make the probabilities slightly higher. (If one of the decays is to $e\overline{\nu_e}\nu_L$, the probabilities are lower.) If the lifetimes are long enough, the trigger problem can be avoided by looking for events in which one or both of the leptons live long enough to be directly observed. Another possibility would be to use

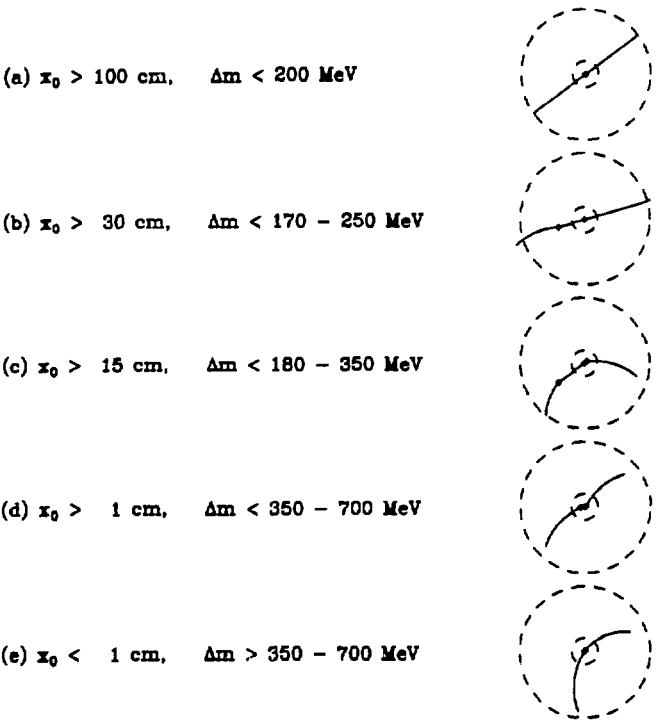

Figure 6.2: Schematic drawings of typical heavy lepton events for various ranges of Δm. Straight lines are heavy leptons, curved lines are their low-energy daughters, and diamonds mark decays. The dashed circles represent the inner and outer radii of the TPC.

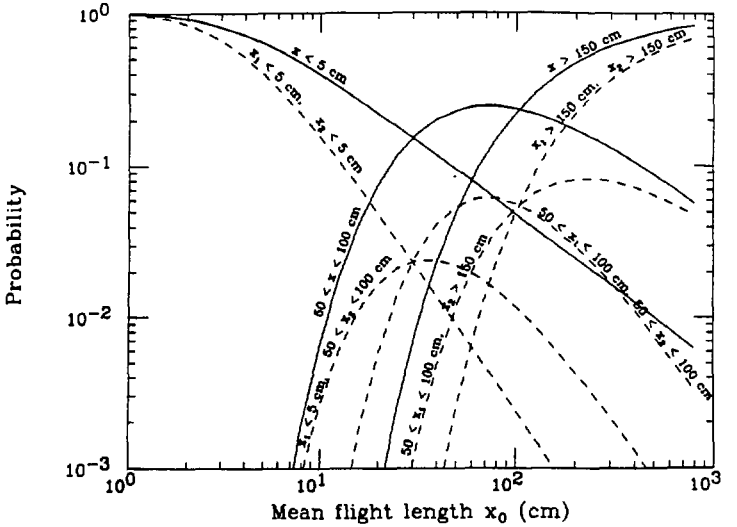

Figure 6.3: Probability that a heavy lepton will decay near the vertex, in the TPC, or outside the TPC, as a function of its mean flight distance x_0. The dashed curves give joint probabilities for both leptons to decay in specified regions.

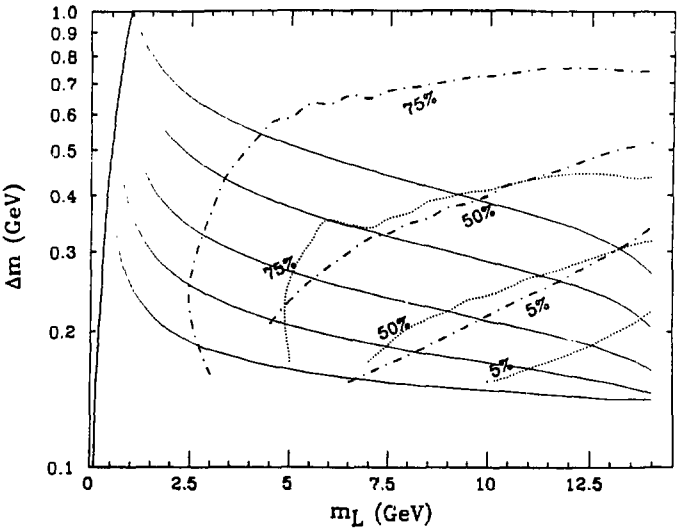

Figure 6.4: Contours of the fraction of two-pion events in which both pions have $p_\perp$ above 350 MeV (solid lines), or above 200 MeV (dotted lines).

TPC data from 1983, which was taken with a lower (3.9 kG) magnetic field. For these Experiments the trigger $p_\perp$ threshold was about 200 MeV, which would give the dashed curves shown in Figure 6.4. This has not yet been tried.

Decay branching ratios in the low Δm region are fairly constant at about 93% π/μ, 7% electrons, for $\Delta m > m_\pi$. The region $\Delta m < m_\pi$ where almost all the decays are $L^- \rightarrow e^- \nu_L \overline{\nu_e}$, is also the region where $x_0 > 100$ cm. In that region it's better to search for long lived leptons.

6.2 Three Searches, and Results

Three ways to look for new leptons at low Δm were considered. The type of events they look for correspond to the drawings in Figure 6.2(a), (b)and (c), and (d), respectively.

6.2.1 Search for two high energy tracks

This was a search for pairs of stable leptons. Figure 6.5 shows the curves of truncated mean dE/dx (defined in Section 3.2.1) vs $\ln p$ for the five common kinds of particles, and for six examples of heavy leptons. The leptons are produced with the beam energy (or slightly less because of radiative corrections); therefore, they won't populate the whole length of their curves but will be clustered at $p(m_L) = \sqrt{E^2 - m_L^2}$. For each m_L curve in Figure 6.5, its intersection with the dashed curve is the place where heavy lepton events would be clustered.

The curves show that, except for $m_L \approx 9$ GeV, leptons can be found or excluded with dE/dx alone, provided their lifetimes are long enough. At 9 GeV, where the heavy lepton curves cross the standard particle curves, heavy leptons are more difficult to detect. Although the backgrounds from e^+e^- and $\mu^+\mu^-$ events are well-understood, and for the e^+e^- events could also be reduced with cuts on calorimeter energy, the errors on such corrections increase the minimum

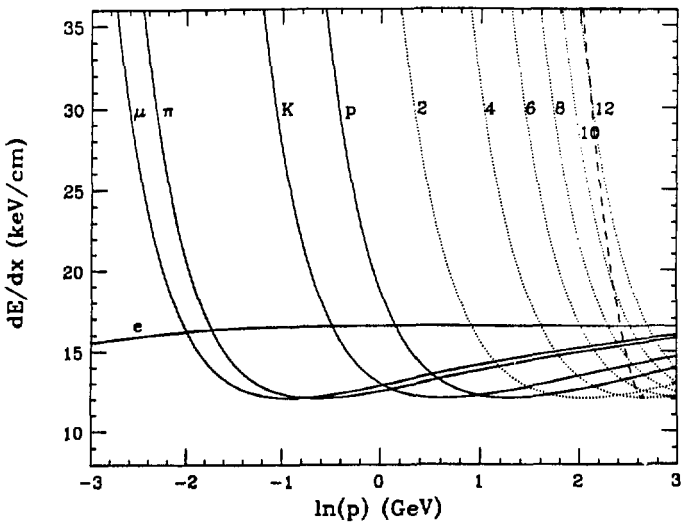

Figure 6.5: dE/dx vs $\ln p$ distributions for common particles and for some examples of heavy particles. Heavy leptons with the 14.5 GeV beam energy would be clustered near the intersection of their mass curve and the dashed curve.

number of L^+L^- events needed for a significant signal, which in turn sharply increases the minimum lifetime that the search is sensitive to. (The usual searches for new stable leptons reduce background except from $\mu^+\mu^-$ events by requiring matching muon chamber hits, but such a requirement triples the distance each lepton is required to travel and so is too severe for moderate lifetime particles.)

For this search, a "two high momentum tracks" subset of the data was selected by requiring that:

1. There were exactly two tracks.
2. Each track came within 6 cm of the beamline and 10 cm of the midplane at its closest approach to the beamline.
3. The momentum of each track was at least 6 GeV.
4. The dip angle of each track was less than 60°.
5. The ripple trigger was satisfied.
6. The event passed charged SelTwoGam cuts (defined in Section 4.1.2).

For comparison, sets of Monte Carlo events were also generated, using the Fast Monte Carlo (FMC), at ten m_L points, and with the leptons given infinite lifetime. Figure 6.6 shows the dE/dx vs $\ln p$ distribution of tracks in events passing the above cuts for (a) Monte Carlo events with $m_L = 10$ GeV and (b) data. An event is considered to be consistent with a given m_L if $\chi^2_{m_L} < 8$, where

$$\chi^2_{m_L} = \sum_{track=1}^{2} \left\{ \frac{(p_{track} - p_0)^2}{\sigma^2_{p_0}} + \frac{(dE/dx_{track} - dE/dx_0)^2}{\sigma^2_{dE/dx_0}} \right\},$$

with $p_0 = \sqrt{(E_{beam} - .1)^2 - m_L^2}$, $\sigma_{p_0} = p_0\sqrt{(.015)^2 + (.007p_0)^2}$ (p_0 in GeV), dE/dx_0 given by the (empirical) dE/dx vs $\ln p$ curve for m_L, and $\sigma_{dE/dx_0} = .04 \times dE/dx_0$. (The 0.1 GeV subtracted from E_{beam} is an approximation of the

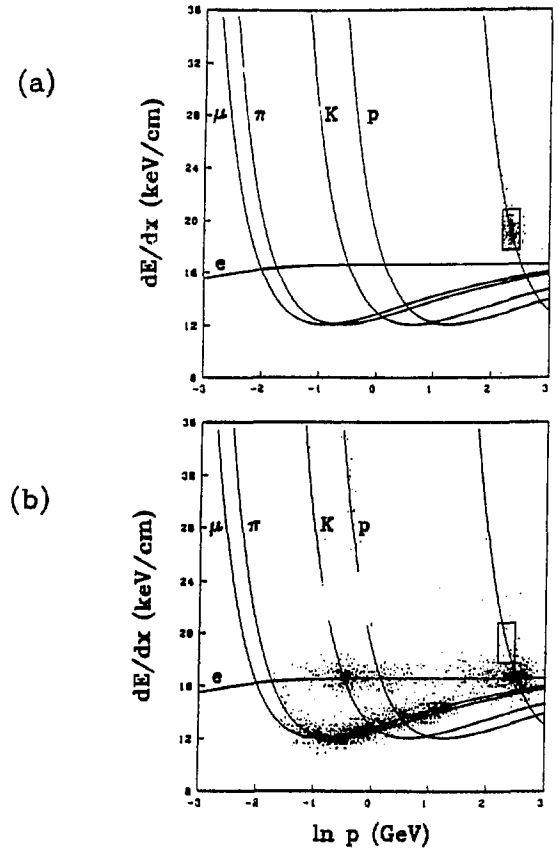

Figure 6.6: dE/dx vs $\ln p$ distributions of tracks in (a) Monte Carlo events with $m_L = 10$ GeV, and (b) data. The right hand curve in each figure is the prediction for $m = 10$ GeV particles and the box is the 2σ limits for particles with $m = 10$ GeV and $E = 14.5$ GeV. (In (b), the cluster of tracks at $\ln p \approx 2.7$ is beam energy electrons.)

average radiative correction.) The box in each figure is the region defined by $|p - p_{m_L}| < 2\sigma_p$, $|dE/dx - dE/dx_0| < 2\sigma_{dE/dx}$, for $m_L = 10$ GeV. The requirement of $\chi^2_{m_L} < 8$ corresponds roughly to requiring both tracks to lie in the appropriate box. (Although there may be quite a few tracks satisfying $\chi^2_{m_L} < 4$, there are far fewer random events with two such tracks.)

The ratio R of the number of observed events to the number of predicted events depends on the cross section for heavy lepton production and on the heavy lepton lifetime:

$$R = \frac{\text{Luminosity} \times \text{cross section}}{\text{number MC generated}} \times (\text{probability of decay outside the TPC})^2,$$

where (probability of decay outside the TPC) $= e^{-x_{outside}/x_0}$. In this study, $x_{outside}$ was set at 150 cm. (The distance through the TPC for a straight track is 100 cm to 141 cm, depending on dip angle, while the distance to the farthest trigger element is 111 cm to 158 cm, so $x_{outside} = 150$ cm is fairly conservative.) Since the cross section is assumed known, an upper limit on R, if it's less than 1, gives an upper limit on x_0.

To set lifetime limits for all m_L, χ^2_m is calculated, for each event, for 70 values of m between .5 GeV and 14.3 GeV. The m values are spaced closely enough that the change in predicted p_0 and dE/dx_0 from one m to the next is much less than σ_{p_0} and σ_{dE/dx_0}; this makes it unimportant exactly which values are used. The number of data events passing all selection cuts and passing $\chi^2_m < 8$ is given as a function of m in Figure 6.7. (Each event can appear in several bins, or not at all.) There were no data events for 1.1 GeV $< m <$ 6.9 GeV and $m >$ 10.8 GeV. As an example of what could be expected from *stable* leptons, the corresponding histogram for Monte Carlo events with $m_L = 6$ GeV is shown in Figure 6.7. For the ten m_L values for which Monte Carlo events were generated, an upper limit on R is calculated as the 95% confidence level upper limit on the number of data points with $\chi^2_{m_L} < 8$, divided by the number of Monte Carlo events with

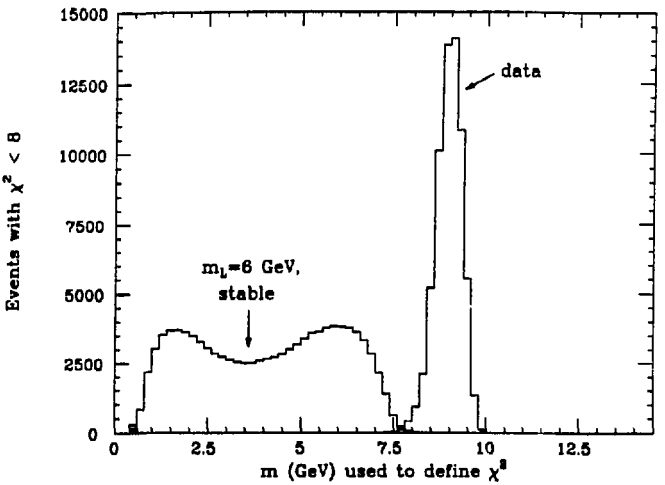

Figure 6.7: Number of data events passing $\chi^2_m < 8$, as a function of the mass m assumed in the definition of χ^2. The histogram for Monte Carlo events with $m_L = 6$ GeV is also shown, scaled to be comparable to the data.

m_L	maximum x_0 (cm)	minimum Δm(GeV)
1	60.6 ± 1.3	.289 ± .002
2	41.9 ± 0.3	.247 ± .001
4	42.1 ± 0.3	.203 ± .001
6	41.9 ± 0.3	.183 ± .001
7	42.4 ± 0.3	.176 ± .001
8	145.0 ± 3.4	.147 ± .001
10	92.5 ± 1.4	.148 ± .001
11	44.8 ± 0.4	.156 ± .001
12	45.3 ± 0.3	.151 ± .001

Table 6.1: Limits on heavy leptons from the two high-energy tracks search.

$\chi^2_{m_L} < 8$. Rearranging the definition of R, this ratio becomes an upper limit on x_0:

$$x_{0,max} = \frac{2x_{outside}}{\ln\left[\frac{\text{Luminosity} \times \text{cross section}}{\text{number of MC events generated} \times R_{max}}\right]}.$$

The lower limit on Δm corresponding to $x_{0,max}$ is then found by interpolation from a table of lifetimes calculated as described in Section 2.3. The results are given in Table 6.1. Because the number of predicted events changes smoothly with m_L, and because the binning in m_L is much narrower than the expected signal, the limits can be interpolated to give the excluded region of Figure 6.8.

6.2.2 Search for one visible decay

To look for leptons with mean flight lengths x_0 in the range 10 cm $< x_0 <$ 100 cm, a search was made for events with one visible decay. A visible decay is one which has TPC tracks fit to both the parent and the daughter. Besides being the most likely topology for 30 cm $< x_0 <$ 100 cm (as can be seen from Figure 6.3), this signature has the advantage of very low background. The only very-high-p to very-low-p transitions expected are from electron bremsstrahlung, and those events are distinguishable from heavy lepton decays because the bremsstrahlung events change the momentum of the track but not its direction. (Sometimes the identification of bremsstrahlung events can also be checked with the calorime-

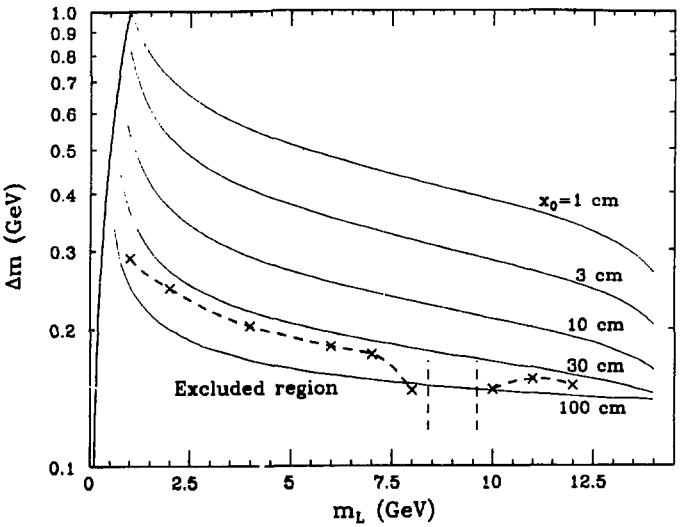

Figure 6.8: Limits on new heavy leptons from the search for long-lived lepton pairs. The boundary of the excluded region lies approximately along the contour $x_0 = 45$ cm. No limits are set for 8.4 GeV $< m_L <$ 9.6 GeV. The x's mark the limits at the m_L values for which Monte Carlo events were generated.

ters.) In K and π decays the track kinks correctly, but the parents have lower momentum and there is less missing energy. Examples of events with the three kinds of decays are displayed in Figure 6.9. In the search, the events were also required to have one other track, which in a heavy lepton event could be either the other heavy lepton if it decays slowly, or a pion if it decays quickly.

One difficulty with this search is that the TPC acceptance for two-track events with decays is borderline, for two reasons:

1. *Triggering.* The small radius - large radius coincidences required by the charged trigger for a ripple track (described in Section 3.3) reject tracks which decay with too large an angle or to a too low-energy daughter. In the $r - z$ plane, the timing of the ripple trigger also discriminates against bent tracks. Both rejections are reinforced by preanalysis (Section 4.2). In order for the searched-for events to trigger, therefore, the decay must be inconspicuous enough to be overlooked by both the trigger and preanalysis.

2. *Pattern recognition.* The pattern-finding algorithm is intentionally biased in favor of long unbroken tracks, and in addition will not find tracks crossing fewer than two (out of the fifteen possible) pad rows. Thus, decays near the edges of the TPC volume and small-angle decays to fairly straight tracks both tend to be badly fit with one track rather than broken into two tracks. This makes them difficult to detect. Even if both tracks are fit, the algorithm often misplaces the decay point, so that the momenta and trajectories of both parent and daughter are unreliable. If the fit to the parent is bad enough, the track (and the event) will also have difficulty later passing vertex cuts.

The combined effect of these two acceptance problems is that while large-angle decays are most likely to be reconstructed, small-angle decays are the only ones

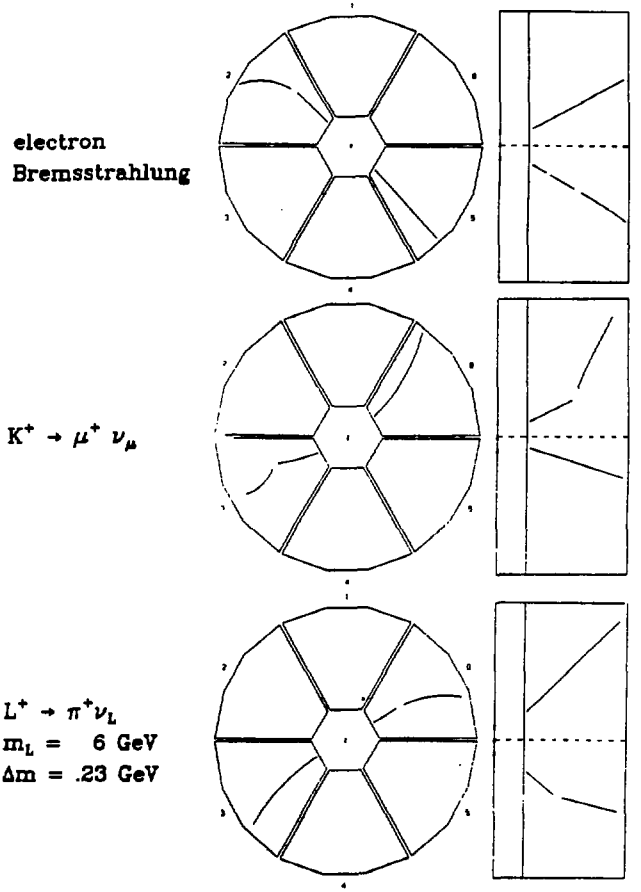

Figure 6.9: Decays as they appear in the TPC: (a) electron Bremsstrahlung event from data (confirmed with dE/dx and calorimeter energy), (b) $K^+ \rightarrow \mu^+\nu_\mu$ event from data (confirmed with dE/dx), and (c) heavy lepton decay from Monte Carlo with $m_L = 6$ GeV, $\Delta m = .23$ GeV.

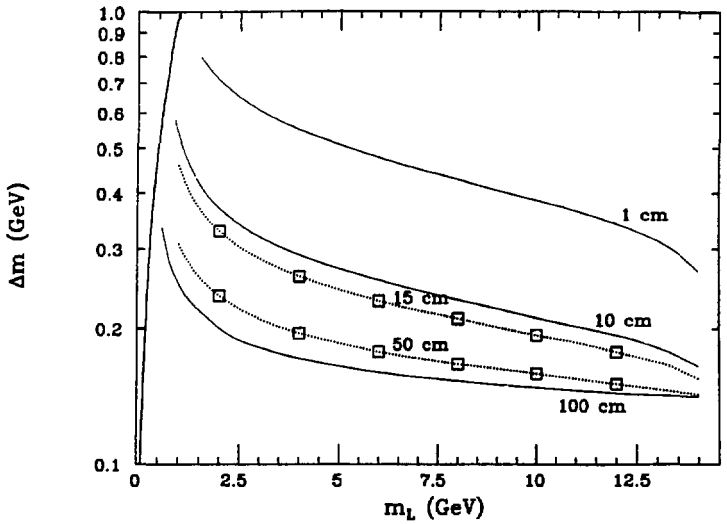

Figure 6.10: Combinations of m_L and Δm for which events were simulated for the two low-energy pions search. They are chosen so that the mean flight distance of the leptons is either 15 cm or 50 cm.

that will trigger. To find out whether the two restrictions overlap or leave an intermediate region where decays (and heavy lepton events) might be seen, heavy lepton events with likely-looking decays were generated with the "slow" Monte Carlo, GLOBAL, which includes a detailed trigger simulation. The events could then be analyzed with the same routines, including the preanalysis, pattern-finding and track-fitting routines, as are used on real data.

The m_L,Δm choices for the Monte Carlo events are shown in Figure 6.10. They were chosen so that half had mean flight paths of $x_0 = 15$ cm, and the other half had $x_0 = 50$ cm. To save computer time, at each m_L,Δm point only two subsets of all the expected heavy lepton events were generated, those with

the L^+ decaying at $x < 5$ cm and the L^- decaying at 50 cm $< x <$ 100 cm, and those with the L^+ decaying at $x > 150$ cm and the L^- decaying at 50 cm $< x <$ 100 cm. This was done by restricting the allowed ranges of x_{L^+} and x_{L^-}, while leaving their distributions within those ranges unchanged. There were 1000 events generated of each type. It was assumed that events not in these subsets (or their charge conjugate) never pass all the event selection cuts.

The requirements for the one visible decay events were:

1. There were exactly three tracks.
2. The event contained a parent, a daughter and a "normal" track, defined as follows:
   (a) Parent track
      i. The track ended in the TPC, between 30 cm and 80 cm from the beamline, and less than 70 cm from the midplane.
      ii. The track momentum was greater than 2 GeV.
   (b) Daughter track
      i. The distance between the end of the parent track and the beginning of the daughter track was less than 30 cm.
      ii. The beginning of the daughter track was more than 30 cm from the beamline.
      iii. The angle between the momentum of the parent at the end of its track and the momentum of the daughter at the beginning of its track was greater than 5.7°.
      iv. The track was not an electron, defined as $\chi^2_e < 4$, $\chi^2_e < \chi^2_{other}$.
   (c) Normal track
      i. The charge of the normal track was opposite that of the daughter.

m_L	Δm	x_0	trigger	3 tracks	all cuts	scale factor	prediction
2	.329	15	341	47	12	.148	1.7
4	.260	15	250	71	40	.147	5.9
6	.230	15	178	66	33	.143	4.7
8	.210	15	88	37	17	.134	2.3
10	.193	15	32	18	7	.121	.8
12	.177	15	3	2	0	.095	0
2	.236	50	349	28	8	.358	2.9
4	.195	50	231	50	20	.345	6.9
6	.177	50	144	50	18	.328	5.9
8	.166	50	62	17	9	.304	2.7
10	.158	50	6	3	1	.269	.3
12	.150	50	0	0	0	.206	0

Table 6.2: Number of events with one visible decay, and one pion from a fast decay.

3. The ripple trigger was satisfied.

4. Charged SelTwoGam cuts were passed.

The parent, daughter, and normal tracks were selected in that order, introducing in theory a slight inefficiency if there happened to be more than one parent candidate in an event, but this happened so rarely that it wasn't a problem.

The results at three stages of the event selection, applied to the 24 Monte Carlo sets (of 1000 events each), are given in Tables 6.2 and 6.3. In the final column, the numbers of Monte Carlo events are scaled to what would be expected in the data. Because the fast-decay and slow-decay event types don't overlap, the *sums* of the final columns of Tables 6.2 and 6.3 can be used for setting limits. Among the real events, there were 549,131 which triggered, 67,424 with three tracks, and none which passed all the cuts.

The results show that only in a small range of m_L,Δm are there enough decays of the accepted type for new leptons to be detected with this kind of search. The limits on the Δm range come mostly from the lifetimes (reflected in the scale factors): at smaller Δm the decays are spread over too large a range of

m_L	Δm	x_0	trigger	3 tracks	all cuts	scale factor	prediction
2	.329	15	79	40	29	2.6×10^{-5}	0
4	.260	15	110	64	38	2.5×10^{-5}	0
6	.230	15	116	64	49	2.4×10^{-5}	0
8	.210	15	117	69	46	2.3×10^{-5}	0
10	.193	15	105	69	47	2.0×10^{-5}	0
12	.177	15	71	34	24	1.6×10^{-5}	0
2	.236	50	95	20	7	.329	2.3
4	.195	50	141	52	31	.315	9.8
6	.177	50	143	58	43	.299	12.9
8	.166	50	124	38	25	.279	7.0
10	.158	50	106	39	27	.248	6.7
12	.150	50	57	24	18	.193	3.5

Table 6.3: Number of events with one visible decay, and one undecayed lepton.

Figure 6.11: TPC wire hits for a simulated heavy lepton decay, with the fitted track (fit to pad hits) superposed.

flight distances, while at larger Δm the flight distances are too short. Within this range, the trigger efficiency is an important limiting factor, especially for events in which both leptons decay. The only recoverable events are the 50-80% which triggered but were rejected because the decay was undetected. Here there is a possibility for improvement, because, as illustrated in Figure 6.11, small angle decays which are missed by the pattern recognition are clearly visible in the wire data. A decay-finding routine using the wires, run near the beginning of the analysis chain, could improve the statistics by maybe a factor of three or four. The Δm region in which the search would be effective, however, would be almost

unchanged by an extra factor of four.

6.2.3 Search for two low-energy pions

Most of the low Δm region is occupied by heavy leptons with mean flight lengths between 1 cm and 15 cm, and which decay predominantly to pions. (The probability of a two-pion event is 80–90%.) A typical event in this region is two low-energy pions, perhaps with poor vertex fits.

There are approximately 130,000 low-energy two-pion/muon events in the TPC data, mostly from the two-photon processes $e^+e^- \rightarrow e^+e^-\mu^+\mu^-$, and $e^+e^- \rightarrow e^+e^-\pi^+\pi^-$. Heavy leptons would be expected to produce between zero and 3000 events, depending on m_L and Δm. The two-photon $\pi^+\pi^-$ cross-section is not understood well enough that a 3% excess of pion pairs could be noticed or excluded. A search for heavy leptons by looking at two-pion events therefore, like the preceding two searches, must be based on the differences between two-photon and heavy lepton pion production, as reflected in the properties of the two-pion events.

For this search, a set of cuts was defined using three techniques: making cuts against known backgrounds, looking for the non-zero lifetime of the heavy leptons, and checking that kinematic constraints on heavy lepton decays are satisfied. As usual, simulated heavy lepton events were generated to check the effect of the cuts, this time for twelve m_L,Δm hypotheses with m_L = 2, 4, 6, 8, 10 and 12 GeV, and Δm = .2 and .3 GeV.

First, basic event requirements were defined as:

1. There were exactly two tracks.

2. The dE/dx identification gave $\chi^2_\pi < 5$ for each track.

3. The ripple trigger was satisfied.

4. The event passed charged SelTwoGam cuts.

Figures 6.12(a) and (b) show distributions of colinearity and coplanarity of the events passing these basic cuts, for data and for three representative heavy lepton hypotheses. The distributions are scaled so that the numbers can be compared directly, but notice the difference in vertical scales. Also, the number of real events in the highest bin of the colinearity and coplanarity histograms is far off-scale. Comparing the distributions, "anti-background" cuts were defined as:

1. The momentum of each pion must be less than 4 GeV, to remove $e^+e^- \rightarrow \mu^+\mu^-$ events.

2. The colinearity angle must be between 120° and 176°, to remove cosmic rays.

3. The coplanarity angle must be between 120° and 177°, to remove two-photon events.

Fig. 6.12(c) shows the distribution of the distance between the two pion tracks at their closest approaches to the beamline, for the events remaining after the anti-background cuts. To further reduce the background, a minimum distance cut was made next, to select events in which the pions might have come from decays and reject events in which both pions were produced at the vertex. Since the mean flight distance x_0 varies strongly with Δm and m_L, defining a single cut is probably not the best procedure, but for this test study a "non-vertex" cut was defined by requiring: distance $\geq$ 2 cm. The number of events remaining after this cut was 1472 in the data and ranged from 6 to 953 in the samples of simulated events; the numbers of events surviving successive cuts are given in Table 6.4.

Finally, each event was checked for consistency with each of the twelve (m_L,Δm) hypotheses. (At this point the cuts stop being independent of m_L

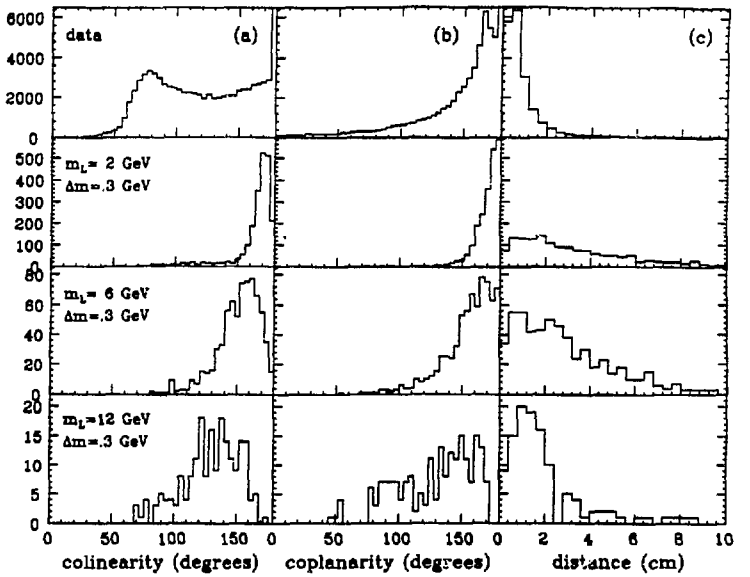

Figure 6.12: Colinearity, coplanarity, and distance distributions of two-pion events. The "distance" is the distance between the two tracks at their closest approaches to the beamline; the distance distribution is shown only for two-pion events which have passed colinearity, coplanarity and momentum cuts. Distributions for data and for three Monte Carlo samples are shown.

m_L	Δm	all	basic cuts	anti-background	non-vertex
2	.3	9200	2175	1562	953
4	.3	8700	1665	1376	828
6	.3	8300	1184	956	576
8	.3	7750	778	600	291
10	.3	6950	468	316	118
12	.3	5500	219	125	39
2	.2	9200	473	322	256
4	.2	8700	628	527	454
6	.2	8300	478	435	382
8	.2	7750	288	256	220
10	.2	6950	86	76	70
12	.2	5500	6	6	6
data		> 835000	127161	19008	1472

Table 6.4: Numbers of "two low energy pion" events passing cuts.

and Δm.) The consistency check makes use of the fact that $L \to \pi\nu_L$ is a two-body decay, so that there are a limited number of degrees of freedom. In fact, a (non-radiative) heavy lepton event can be completely described with ten parameters: m_L, Δm, L^+ production angles θ_L and ϕ_L, L^+L^- flight distances x^+, x^-, and center of mass decay angles θ^+, θ^-, ϕ^+, ϕ^-, while each two-pion event has ten measured parameters, five for each pion helix. In principle, one could, with a knowledge of all measurement errors (and of errors on other "known" values such as the beam position and energy), and in the absence of radiative effects, define exactly a chi-squared for the fit of each event to an m_L, Δm hypothesis. In practice the consistency was checked with a simpler algorithm which joined the two pion helices with a series of straight trial lines (the L^+L^- trajectories). For each line, its closest approach to the nominal interaction point and the angles at which it intersected each pion helix were calculated, and a figure of merit for the line was defined as:

$$f(m_L, \Delta m) = \frac{(x_{closest} - x_{beam})^2}{\sigma_x^2} + \frac{(y_{closest} - y_{beam})^2}{\sigma_y^2} + \frac{(z_{closest} - z_{beam})^2}{\sigma_z^2}$$

$$+ \frac{(\alpha^+ - \alpha_0^+)^2}{\sigma_\alpha^2} + \frac{(\alpha^- - \alpha_0^-)^2}{\sigma_\alpha^2}.$$

The nominal lab frame decay angles $\alpha_0^\pm$ are calculated for each track from m_L, Δm, E_{beam}, and $p_{\pi^\pm}$. The errors, estimated from the momentum resolution for 1 GeV tracks and from the beam position variance, were set at σ_x = .4 cm, σ_y = .4 cm, σ_z = 1.6 cm, and σ_α = 1°. The line with the minimum value of $f \equiv f_{min}$ was chosen as the best fit to the m_L, Δm hypothesis. Figure 6.13 shows an example of how well this algorithm reconstructs the correct (generated) decays when it is given the correct m_L,Δm hypothesis. (In this example, m_L is 6 GeV, Δm is .3 GeV, and f_{min} is 1.95.) Figure 6.14 shows the distribution of $f_{min}(m_L = 6, \Delta m = .3)$ for (a) simulated events with m_L = 6 GeV, Δm = .3 GeV, and (b) data. (The events with large f_{min} are probably radiative events, which are expected to be poorly fit.)

The number of data events passing all selection cuts and consistent with a given m_L,Δm (defined by $f_{min}(m_L, \Delta m) < 10$) is shown in Figure 6.15 for two values of Δm and as a function of the hypothesized m_L used to calculate f. The solid curves in the figure are Monte Carlo results, labeled with the *generated* lepton mass. The results show that leptons with $m_L < 8$ GeV and $\Delta m \approx .3$ GeV might be excluded with a search of this type.

6.3 Summary of Small Δm Results

The combined results of the three small Δm studies are shown in Figure 6.16. In the figure, x's mark the m_L,Δm points where the Monte Carlo predicted more events than were found in the data. Open diamonds and squares mark points at which, respectively, the two low-energy pions and one visible decay searches were not effective. The shaded regions are *guesses*, based on this study, of the limits that might be set with these two search techniques. To determine the boundaries exactly would require generating considerably more Monte Carlo events, and a

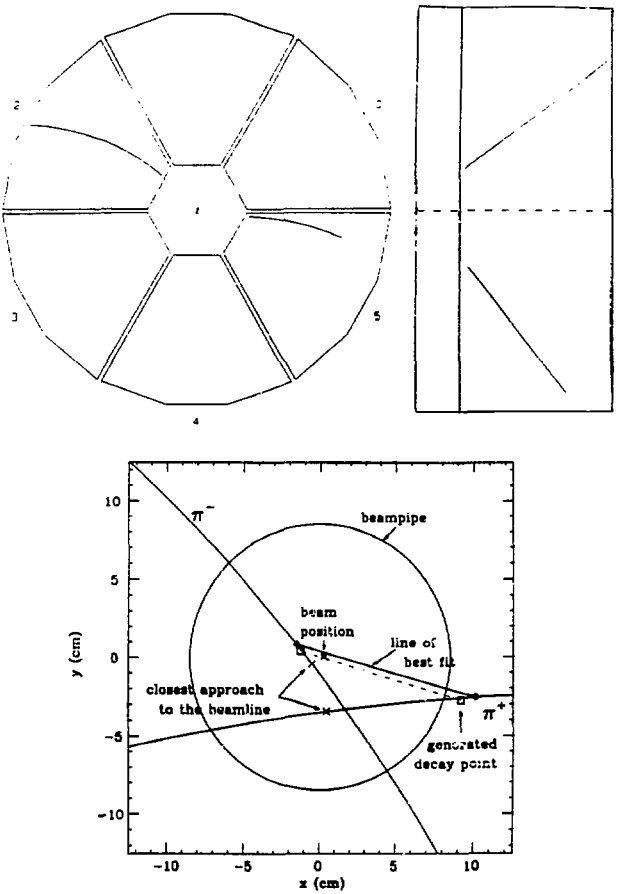

Figure 6.13: A Monte Carlo heavy lepton event as it appears in the TPC (top) and an enlargement showing the extrapolated tracks near the beamline. The dashed line is the generated L^+ and L^- trajectories, while the solid line is the result of the fitting algorithm. (In this particular event the fit is slightly off because the L^+L^- pair happened to be generated at $z = 2.1$ cm.)

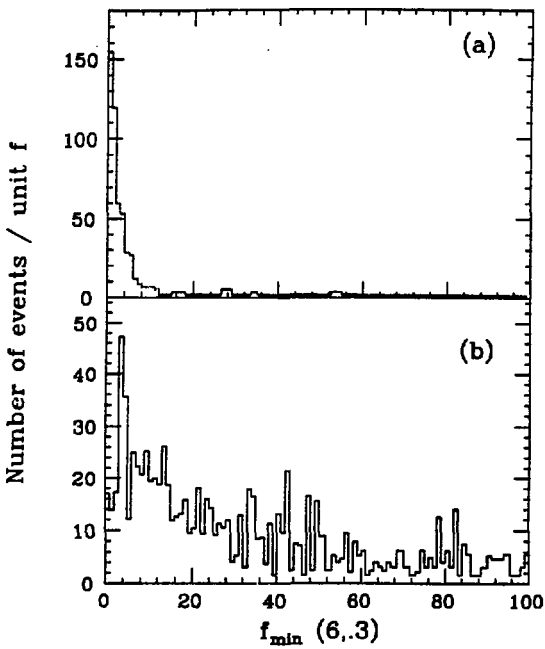

Figure 6.14: Distribution of the figure of merit f_{min} of the fit of two-pion events to the hypothesis that they come from decays of heavy leptons with $m_L = 6$ GeV, $\Delta m = .3$ GeV. The distributions are shown for (a) Monte Carlo events generated with $m_L = 6$ GeV, $\Delta m = .3$ GeV, and (b) data.

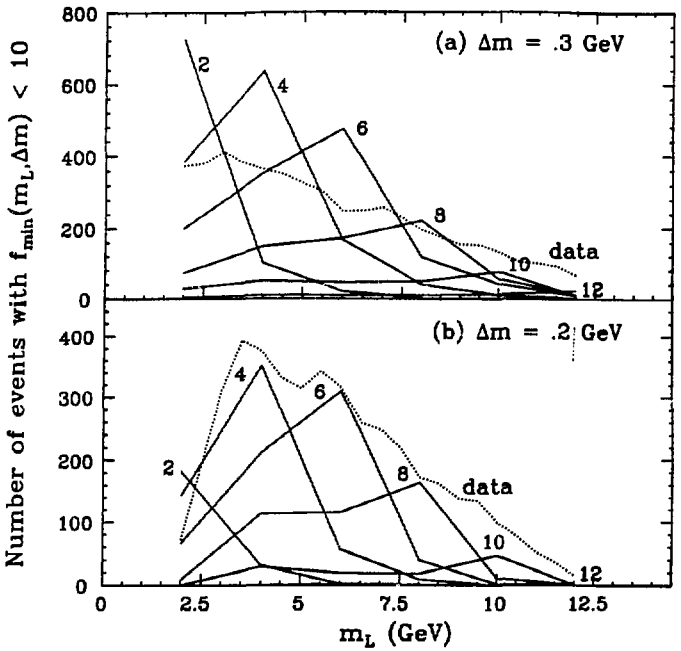

Figure 6.15: Number of events satisfying $f_{min}(m_L, \Delta m) < 10$, as a function of m_L and for two values of Δm. The dotted line is data, and the solid lines are the results for Monte Carlo events. The Monte Carlo curves are labeled with the m_L used to generate them, and the generated Δm is the same as the hypothesized Δm used to define f (i.e. .3 GeV in (a) and .2 GeV in (b)).

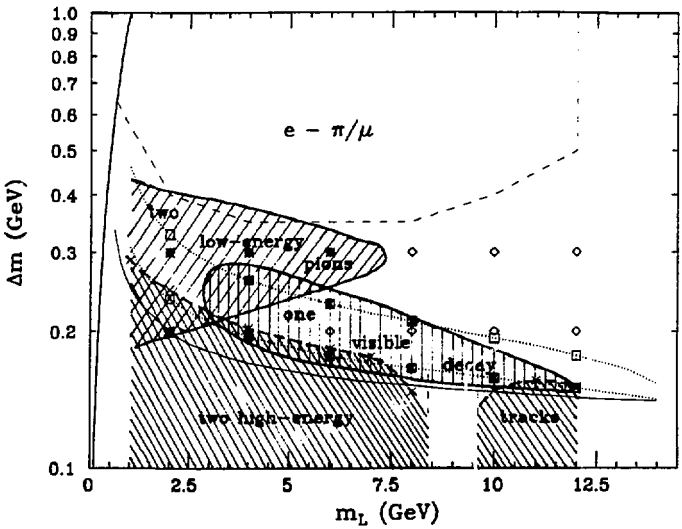

Figure 6.16: *Approximate* boundaries of the m_L,Δm regions that can be checked with the two low-energy pions and one visible decay searches, and the region excluded by the search for two high-energy tracks.

careful study of the reliability of the Monte Carlo predictions for these types of events. Of course, the effects of systematic errors have not been included here, and those of statistical errors are only approximated.

The boundary of the region labeled "two high-energy tracks" (the stable lepton search) has been more carefully determined. Except in the range 8.4 GeV $< m_L <$ 9.6 GeV, it may be considered a preliminary limit on heavy leptons with mean flight distances of more than 45 cm at 14.5 GeV, and as a confirmation of the exclusion of heavy leptons with mean flight distances of more than a meter at 22.5 GeV.

Chapter 7

Summary and Conclusions

If there is a fourth generation of leptons, then the characteristics of L^+L^- pairs produced in e^+e^- collisions depend not only on the mass of the charged leptons, but on the mass of the associated neutrinos. Searches which assume that the fourth generation neutrinos have zero mass cannot be used to set limits on new leptons associated with neutrinos of any mass.

This thesis describes searches made with the TPC/2γ detector specifically for new leptons with massive neutrinos. The properties of these leptons were predicted by combining the theory of weak interactions with the measured properties of the first three lepton generations. Four searches were then designed, optimized for different combinations of the charged lepton mass, m_L, and the neutrino mass, m_{ν_L}.

The best search technique was to look for two-particle electron – pion (or muon) events from the decays $L^- \rightarrow e^-\overline{\nu}_e\nu_L$, $L^+ \rightarrow \pi^+\overline{\nu}_L$ or $L^+ \rightarrow \mu^+\nu_\mu\overline{\nu}_L$ (or the charge conjugates). Comparing the numbers of predicted events with the measured numbers of events, no evidence was found for new heavy leptons, and the possibility of new leptons with $m_L < 12$ GeV and 0.4 GeV $< m_L - m_{\nu_L} <$ 2.5 GeV (approximately) was ruled out at the 99% confidence level. Figure 7.1 shows the boundaries of this limit on new leptons in region G, and limits from previous experiments in regions A through F.

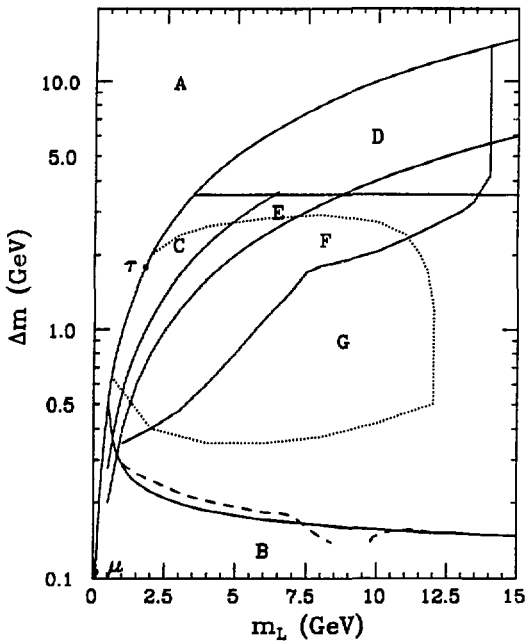

Figure 7.1: Regions of m_L,Δm where new leptons are excluded: region A by definition, regions B through F by other experiments, and region G by the $e - \pi/\mu$ search of this experiment. Also shown is the preliminary limit from the search for long-lived leptons, which excludes the region below the dashed line.

A study was also conducted of ways to look with the TPC for new leptons when the difference between m_L and m_{ν_L} is very small, less than 0.4 GeV. In this region the characteristics of L^+L^- events change very rapidly with m_L and m_{ν_L}, and each search method can only be applied to a limited range of m_L and m_{ν_L}. It was found that three methods combined might cover about half the $\Delta m < 0.4$ GeV, $m_L < 12$ GeV region, as shown in Figure 6.16. The preliminary result of one of these searches, for long-lived leptons, is that new leptons in the region below the dashed line of Figure 7.1 are excluded at the 95% confidence level, with statistical errors only. Preliminary versions of the other two searches also found no new leptons, but limits cannot be set without a more careful determination of the precise boundaries of the resulting excluded regions. These searches were not continued beyond the level of a study because the regions in which they are effective are rather small, and because of the good prospects for searching for these leptons with future experiments.

Bibliography

[1] M.L. Perl *et al. Phys. Rev. Lett.* **35**, 1489 (1975).

[2] K.K. Gan and M.L. Perl. SLAC Report SLAC-PUB-4331, November 1987.

[3] H. Harari. Electroweak interactions – standard and beyond. In Eileen C. Brennan, editor, *Probing the Standard Model, Proceedings of the Fourteenth SLAC Summer Institute on Particle Physics*, page 1, Stanford, CA, July 1986.

[4] M.L. Perl. Heavy leptons in 1986. In S.C. Loken, editor, *Proceedings of the XXIII International Conference on High Energy Physics*, page 596, Berkeley, CA, July 1986.

[5] S. Raby and G.B. West. *Nucl. Phys. B* **292**, 793 (1987).

[6] W. Bartel *et al.*, JADE. *Z. Phys. C* **29**, 505 (1985).

[7] W. Bartel *et al.*, JADE. *Phys. Lett.* **152B**, 392 (1985).

[8] Particle Data Group. *Phys. Lett.* **170B**, 1 (1986).

[9] I. Adachi *et al.*, TOPAZ. *Phys. Rev. D* **37**, 1339 (1988).

[10] H.Yoshida *et al.*, VENUS. *Phys. Rev. Lett.* **59**, 2915 (1987).

[11] B. Adeva *et al.*, MARKJ. *Phys. Rev. Lett.* **48**, 967 (1982).

[12] C. Albajar *et al.*, UA1. *Phys. Lett.* **185B**, 241 (1987).

[13] R.M. Barnett and H.E. Haber. *Phys. Rev. D* **36**, 2042 (1987).

[14] T.L. Lavine. The bound on the number of neutrinos from $e^+e^- \to \gamma\nu\bar{\nu}$ at PEP and PETRA. In E.C. Brennan, editor, *Probing the Standard Model, Proceedings of the Fourteenth SLAC Summer Institute on Particle Physics*, page 49, Stanford, CA, July 1986.

[15] C. Albajar *et al.*, UA1. *Phys. Lett.* **198B**, 271 (1987).

[16] R. Ansari *et al.*, UA2. *Phys. Lett.* **186B**, 440 (1987).

[17] F. Halzen and K. Mursula. *Phys. Rev. Lett.* **51**, 857 (1983).

[18] D.P. Stoker and M.L. Perl. Search for close-mass lepton pairs (L^-, L^0). In J. Tran Thanh Van, editor, *Proceedings of the 22nd Rencontre de Moriond, Vol. 1*, page 45, Les Arcs, Savoie, France, March 1987.

[19] E. Simopoulou. Neutrino counting by measuring $\sigma(e^+e^- \to \gamma\nu\bar{\nu})$ at LEP. In J. Ellis and R. Peccei, editors, *Physics at LEP, (CERN 86-02 Vol. 1)*, page 197, Geneva, February 1986.

[20] F.A. Berends *et al. Nucl. Phys.* **B202**, 63 (1982).

[21] F.A. Berends and R. Kleiss. *Nucl. Phys.* **B178**, 141 (1981).

[22] F.A. Berends *et al. Acta Phys. Pol.* **B14**, 413 (1983).

[23] Y.S. Tsai. *Phys. Rev. D* **4**, 2821 (1971).

[24] F.J.Gilman and S.H. Rhie. *Phys. Rev. D* **31**, 1066 (1985).

[25] F.J.Gilman and D.H. Miller. *Phys. Rev. D* **17**, 1846 (1978).

[26] L.B. Okun. *Leptons and Quarks.* North Holland Publishing Co., Amsterdam, 1982.

[27] Y.S. Tsai. *Phys. Rev. D* **19**, 2809 (1979).

[28] Y.S. Tsai. SLAC Report SLAC-PUB-2450, December 1979.

[29] R.E. Shrock. *Phys. Rev. D* **24**, 1275 (1981).

[30] D.P. Stoker, private communication.

[31] H. Kolanoski. *Two-Photon Physics at e^+e^- Storage Rings.* Springer-Verlag, Berlin, 1984.

[32] W.G.J. Langeveld. *Pion and Kaon pair-production in photon-photon collisions.* PhD thesis, Utrecht, 1985.

[33] H. Aihara *et al.* LBL Report LBL-23737, 1987.

[34] H. Aihara *et al. IEEE Trans. Nucl. Sci.* **NS-30**, 153 (1983).

[35] J.W. Gary. *Tests of Models for Parton Fragmentation in e^+e^- Annihilation.* PhD thesis, Univ. of California, Berkeley, 1985.

[36] H. Aihara *et al. IEEE Trans. Nucl. Sci.* **NS-30**, 67 (1983).

[37] M.T.Ronan. TPC note TPC-LBL-87-12, May 1987.

[38] F.C.Ernè *et al.* TPC note TPC-TWG-85-1, April 1985.

[39] M.T.Ronan. TPC note TPC-LBL-87-15, June 1987.

[40] M.T.Ronan. TPC note TPC-LBL-87-14, June 1987.

[41] R. Bhattacharya *et al. Phys. Rev. D* **15**, 3267 (1977).

[42] J. Smith *et al. Phys. Rev. D* **15**, 3280 (1977).

[43] J.A.M. Vermaseren *et al. Phys. Rev. D* **19**, 137 (1979).

[44] F.A. Berends and R. Kleiss. *Comp. Phys. Comm.* **29**, 185 (1983).

[45] K.A. Derby. TPC note TPC-LBL-87-17, May 1987.